Article

Cell Metabolism

PPARγ Links BMP2 and TGFβ1 Pathways in Vascular Smooth Muscle Cells, Regulating Cell Proliferation and Glucose Metabolism

Graphical Abstract

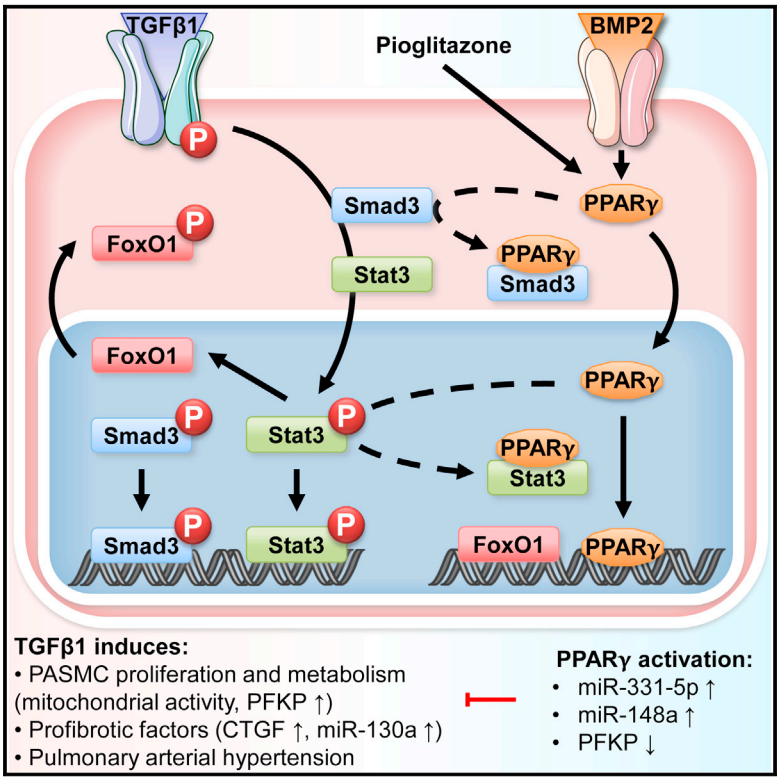

Highlights

- Downstream of BMP2, PPARγ inhibits TGFβ1-Smad3/4 and TGFβ1-Stat3-FoxO1 axis
- TGFβ1 decreases PPARγ via miR-130a/301b in human and murine pulmonary artery SMC
- PPARγ inhibits TGFβ1-induced glucose metabolism (PFKP via miR331-5p, mito activity)
- TGFβ1-overexpressing mice develop PAH that is reversed by PPARγ agonist treatment

Authors

Laurent Calvier, Philippe Chouvarine, Ekaterina Legchenko, ..., Danny Jonigk, Miklos M. Mozes, Georg Hansmann

Correspondence

georg.hansmann@gmail.com

In Brief

Calvier et al. identify PPARγ as a missing link between pro-proliferative TGFβ1 and anti-proliferative BMP2 signaling in vascular smooth muscle cells. The BMP2 downstream effector PPARγ binds to Smad3/Stat3, and inhibits TGFβ1-induced glucose metabolism and pulmonary arterial hypertension (PAH). PPARγ activation by pioglitazone reverses PAH in mice.

Calvier et al., 2017, Cell Metabolism *25*, 1118–1134
May 2, 2017
http://dx.doi.org/10.1016/j.cmet.2017.03.011

CellPress

PPARγ Links BMP2 and TGFβ1 Pathways in Vascular Smooth Muscle Cells, Regulating Cell Proliferation and Glucose Metabolism

Laurent Calvier,[1] Philippe Chouvarine,[1] Ekaterina Legchenko,[1] Nadine Hoffmann,[1] Jonas Geldner,[1] Paul Borchert,[1] Danny Jonigk,[2] Miklos M. Mozes,[3] and Georg Hansmann[1,4,*]
[1]Department of Pediatric Cardiology and Critical Care
[2]Institute of Pathology
Hannover Medical School, Hannover 30625, Germany
[3]Department of Pathophysiology, Semmelweis University, Budapest 1089, Hungary
[4]Lead Contact
*Correspondence: georg.hansmann@gmail.com
http://dx.doi.org/10.1016/j.cmet.2017.03.011

SUMMARY

BMP2 and TGFβ1 are functional antagonists of pathological remodeling in the arteries, heart, and lung; however, the mechanisms in VSMCs, and their disturbance in pulmonary arterial hypertension (PAH), are unclear. We found a pro-proliferative TGFβ1-Stat3-FoxO1 axis in VSMCs, and PPARγ as inhibitory regulator of TGFβ1-Stat3-FoxO1 and TGFβ1-Smad3/4, by physically interacting with Stat3 and Smad3. TGFβ1 induces fibrosis-related genes and miR-130a/301b, suppressing PPARγ. Conversely, PPARγ inhibits TGFβ1-induced mitochondrial activation and VSMC proliferation, and regulates two glucose metabolism-related enzymes, platelet isoform of phosphofructokinase (PFKP, a PPARγ target, via miR-331-5p) and protein phosphatase 1 regulatory subunit 3G (PPP1R3G, a Smad3 target). PPARγ knockdown/deletion in VSMCs activates TGFβ1 signaling. The PPARγ agonist pioglitazone reverses PAH and inhibits the TGFβ1-Stat3-FoxO1 axis in TGFβ1-overexpressing mice. We identified PPARγ as a missing link between BMP2 and TGFβ1 pathways in VSMCs. PPARγ activation can be beneficial in TGFβ1-associated diseases, such as PAH, parenchymal lung diseases, and Marfan's syndrome.

INTRODUCTION

Transforming growth factor β (TGFβ) pathways are critical for tissue homeostasis and contain multiple layers, including cyclin-dependent kinase (CDK)-mediated phosphorylation of Smad3 (Alarcón et al., 2009), and bone morphogenetic proteins (BMPs) (Akhurst and Hata, 2012; Long et al., 2015; Morrell et al., 2016)—a crosstalk mainly described for BMP9 in endothelial cells (Long et al., 2015). In the cardiovascular-pulmonary system, TGFβ1 signaling induces fibroblast and smooth muscle cell (SMC) proliferation, inflammation, endothelial-mesenchymal transition (EnMT), and fibrosis (Akhurst and Hata, 2012; Calvier et al., 2013, 2015; Chen et al., 2016; Xu et al., 2012)—all hallmarks of pulmonary arterial hypertension (PAH) (Hassoun et al., 2009; Ranchoux et al., 2015; Sheikh et al., 2014; Tuder et al., 2013).

TGFβ1 was found to be elevated in plasma (Selimovic et al., 2009) and pulmonary artery SMCs (PASMCs) from PAH patients (Ma et al., 2011), and in rodent models of PAH (monocrotaline and chronic hypoxia) (Long et al., 2009; Yung et al., 2016; Zaiman et al., 2008). Inhibition of TGFβ receptor type 1 (TGFBR1) or TGFβ1 attenuates pulmonary vascular remodeling and right ventricular (RV) hypertension in these animal models (Long et al., 2009; Yung et al., 2016; Zaiman et al., 2008). Through TGFBR1 and TGFBR2 activation, TGFβ1 phosphorylates Smad2 and 3, which form complexes with co-Smad4 that translocate into the nucleus to regulate gene transcription (canonical pathway) and microRNA (miRNA) biosynthesis (Akhurst and Hata, 2012; Macias et al., 2015; Xu et al., 2012).

Importantly, dysfunction or loss-of-function mutations of BMP receptor 2 (BMPR2), another TGFβ superfamily member, are frequently found in hereditary, idiopathic, and other forms of PAH (Barnes et al., 2016; Long et al., 2009; Soubrier et al., 2013). BMP signaling is crucial for cardiovascular homeostasis and metabolic regulation (Morrell et al., 2016; Sutendra and Michelakis, 2014), through preservation of endothelial mitochondrial metabolism (Diebold et al., 2015) and prevention of EnMT (Hopper et al., 2016), which are frequently disturbed in PAH. BMP2, through its receptor, BMPR2, counteracts the TGFβ1-TGFBR pathway (Feng et al., 2016; Morrell et al., 2016); however, the underlying mechanisms of the downstream crosstalk, especially in vascular SMCs (VSMCs), are incompletely understood.

Peroxisome proliferator-activated receptor gamma (PPARγ) is a nuclear hormone receptor and transcription factor that plays a major beneficial role in cardiovascular homeostasis (Pelham et al., 2012) and glucose metabolism (Banks et al., 2015). Moreover, PPARγ regulates multiple genes and co-factors implicated in the pathobiology of PAH (Ameshima et al., 2003; Hansmann and Zamanian, 2009). Previously, we discovered that vasoprotective PPARγ acts downstream of BMP2-BMPR2 (Hansmann et al., 2008), and that its deletion in murine SMCs results in

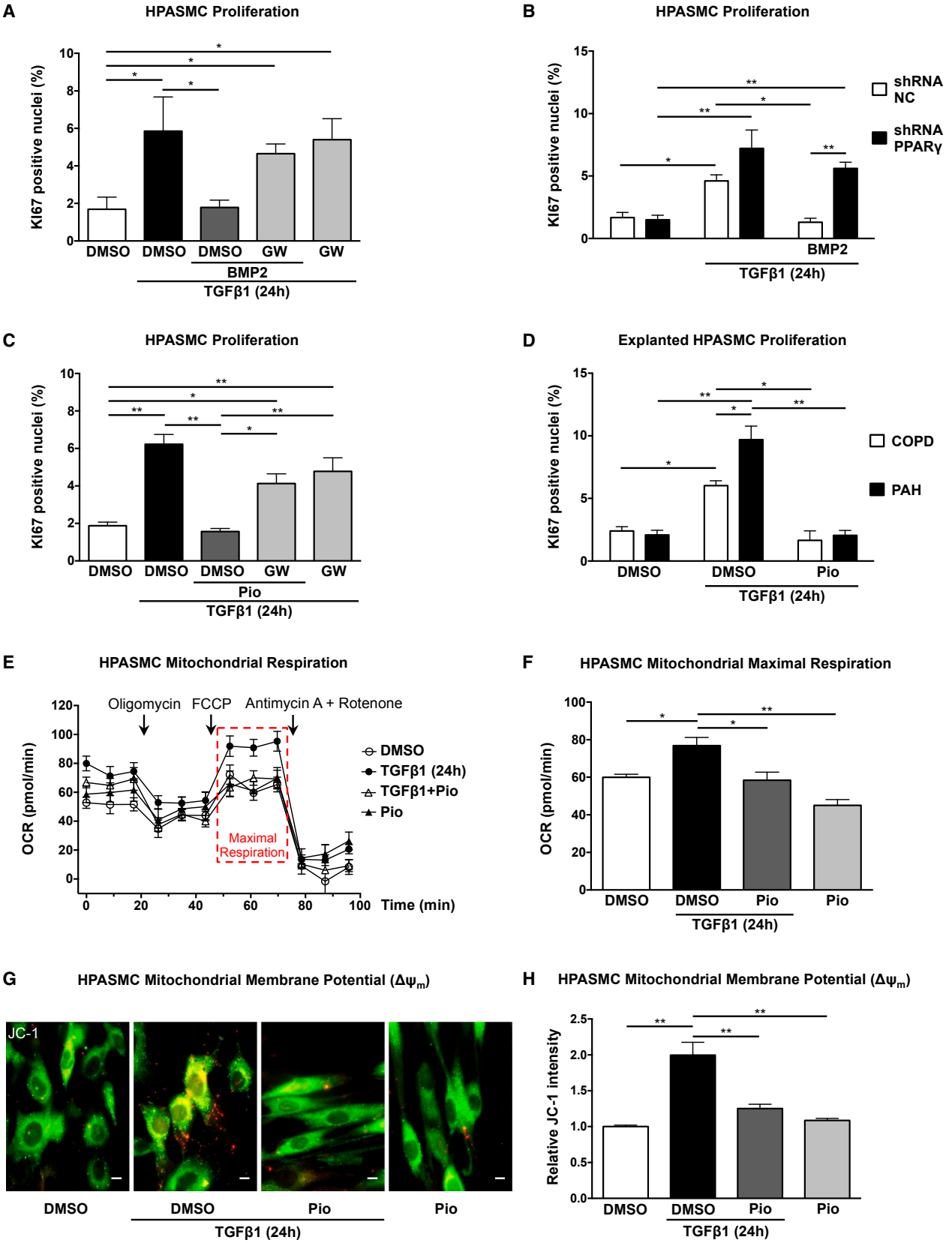

(legend on next page)

PAH, RV hypertrophy (RVH), and pulmonary artery remodeling in vivo. In PAH-PASMCs and in PAH rat models, activation of transducer and activator of transcription 3 (Stat3) by advanced glycation end-product receptor (RAGE) decreases BMPR2-PPARγ signaling, leading to PAH (Meloche et al., 2013).

So far, the mechanisms of the TGFβ1-BMP2 balance (functional antagonism) in VSMCs, and its disturbance in PAH, are unclear. We hypothesized that PPARγ is an important missing link between anti-proliferative BMP2 and growth-promotive TGFβ1 pathways in murine and human VSMCs (HVSMCs). We identified a pro-proliferative TGFβ1-Stat3-Forkhead box O1 (FoxO1) axis in VSMCs, and PPARγ as regulator of both the canonical Smad3/4 and the non-canonical Stat3-FoxO1 pathway, by physically interacting with Smad3 and Stat3 (Figure S1). TGFβ1 induced both fibrosis-related gene expression and miR-130a/301b, thus decreasing PPARγ. Conversely, PPARγ inhibited TGFβ1-induced mitochondrial activation and regulated the expression of two glucose metabolism-related enzymes, platelet isoform of phosphofructokinase (PFKP, a PPARγ target) and protein phosphatase 1 regulatory subunit 3G (PPP1R3G, a Smad3 target), as well as miR-331-5p, which is predicted to decrease PKFP expression. The PPARγ agonist pioglitazone fully reversed PAH and RVH in TGFβ1-overexpressing mice and inhibited the TGFβ1-Stat3-pFoxO1 axis in vivo.

RESULTS

PPARγ Activation Inhibits TGFβ1-Induced HPASMC Proliferation and Mitochondrial Activity

To assess TGFβ1-induced HPASMC proliferation and its regulation by pharmacological PPARγ activation, we quantified nuclear Ki67 expression as a surrogate for HPASMC proliferation (Figures 1A–1D); as complementary methods, cell count, crystal violet, and MTT absorbance assays were performed and revealed similar results (Figure S2). Recombinant BMP2 inhibited TGFβ1-induced proliferation of HPASMCs, an effect that was absent in the presence of the irreversible PPARγ antagonist GW9662 (Figures 1A and S2A–S2C). In PPARγ knockdown cells, BMP2 failed to inhibit TGFβ1-induced proliferation (Figures 1B, S3D, and S3E), suggesting that BMP2 inhibits the mitogenic effect of TGFβ1 through PPARγ activation.

To validate the inhibitory effect of the PPARγ agonist pioglitazone on TGFβ1-mediated proliferation, we showed that pioglitazone completely inhibited TGFβ1-induced proliferation of control HPASMCs (Figures 1C and S2D–S2F). TGFβ1 induced stronger proliferation in isolated explant HPASMCs from PAH patients than in control chronic obstructive pulmonary disease (COPD) HPASMCs, and such proliferation was abolished by pioglitazone (Figures 1D, S2G, and S2H). The antiproliferative effect of pioglitazone was PPARγ mediated since co-incubation of pioglitazone with the irreversible PPARγ antagonist GW9662 preserved TGFβ1-induced proliferation (Figures 1C and S2D–S2F).

Beyond proliferation, we assessed mitochondrial respiration directly by measuring the oxygen consumption rate (OCR) (Figure 1E), maximal respiration (Figure 1F), and hyperpolarization of mitochondrial membrane potential (Figures 1G and 1H) that occur in myointimal hyperplasia (Deuse et al., 2014). TGFβ1 increased maximal respiration, which was blocked by pre-incubation with pioglitazone (Figure 1F). To confirm this result, we quantified the mitochondrial transmembrane potential, reflecting mitochondrial activation, by JC-1 fluorescence (red-yellow/green fluorescence ratio), in response to TGFβ1 (Figures 1G and 1H). TGFβ1-induced mitochondrial activation was fully inhibited by pre-incubation with pioglitazone (Figure 1H). Taken together, these data support the role of PPARγ as an inhibitor of TGFβ1-induced proliferation and mitochondrial activation in HPASMCs.

PPARγ Activation Inhibits the TGFβ1 Canonical Phosphorylation Cascades Smad3/4

To explain the functional antagonistic effect of BMP2-PPARγ on TGFβ1-induced proliferation, we next investigated to what extent PPARγ could inhibit canonical TGFβ1 signaling in HPASMCs. In response to TGFβ1, a 19-fold increase in phospho-Smad3 (pSmad3) was observed at 30 min in total cell lysate (Figure S3A). Smad3 phosphorylation was accompanied by shuttling of pSmad3 and Smad4 into the nucleus (Figures 2A–2C), while pre-incubation with pioglitazone inhibited such phosphorylation and shuttling.

To further explore the underlying mechanism of the PPARγ-Smad3/4 inhibition, we tested for any direct interactions of PPARγ with Smad3 or Smad4 by co-immunoprecipitation (coIP). PPARγ, activated by pioglitazone, immunoprecipitated with Smad3 following TGFβ1 stimulation, indicating that active PPARγ binds to TGFβ1-activated Smad3 (Figure 2D). Binding of PPARγ to pSmad3 or Smad4 was not detected (data not shown). PPARγ-Smad3 interaction was validated in reciprocal coIP (Figure S3C). The complementary Duolink assay confirmed and illustrated that the pioglitazone-induced PPARγ binding to Smad3 mainly occurs in the cytoplasm (Figure 2E).

Figure 1. PPARγ Activation, through BMP2 or Pioglitazone, Inhibits TGFβ1-Induced Proliferation and Mitochondrial Respiration of HPASMCs

(A–D) Proliferation was assessed by Ki67 immunofluorescence in HPASMCs starved for 24 hr and pre-incubated as indicated with the PPARγ antagonist GW9662 (1 μM; A and C) or DMSO (volume equivalent) for 1 hr, then with BMP2 (10 ng/mL; A and B) or pioglitazone (10 μM; C and D) for another 24 hr and stimulated with TGFβ1 (5 ng/mL) for 24 hr. HPASMCs were stained for Ki67 and DAPI (nucleus) and considered positive when Ki67 overlapped the nucleus.

(B) Before the stimulations, HPASMCs were transduced using lentiviral constructs with shRNA negative control (NC) or shRNA targeting PPARγ mRNA.

(D) HPASMCs isolated from pulmonary arteries were used, from COPD (chronic obstructive pulmonary disease, as control) or PAH patients (n = 3 experiments).

(E–H) Mitochondrial respiration (oxidative phosphorylation) was measured with Seahorse analyzer (E and F) or JC-1 assay (G and H) in HPASMCs starved and pre-incubated with the PPARγ agonist pioglitazone (10 μM) or DMSO (volume equivalent) for 24 hr, then stimulated with TGFβ1 (5 ng/mL) for another 24 hr.

(E and F) Mitochondrial respiration was assessed directly by measuring the oxygen consumption rate (OCR) with the Seahorse XF Cell Mito Stress test. Data are representative of two independent experiments.

(G and H) The mitochondrial transmembrane potential ($\Delta\psi_m$), reflecting the mitochondrial function and health, was assessed by JC-1 Mitochondrial Membrane Potential assay. Mitochondrial hyperpolarization is indicated by an increase in the red/green fluorescence intensity ratio. Representative pictures are shown on adherent living cells (scale bar, 40 μm) (G). Quantitative quantification was done on living cells in suspension (n = 3 experiments) (H).

All values are expressed as mean ± SEM; *p < 0.05; **p < 0.01.

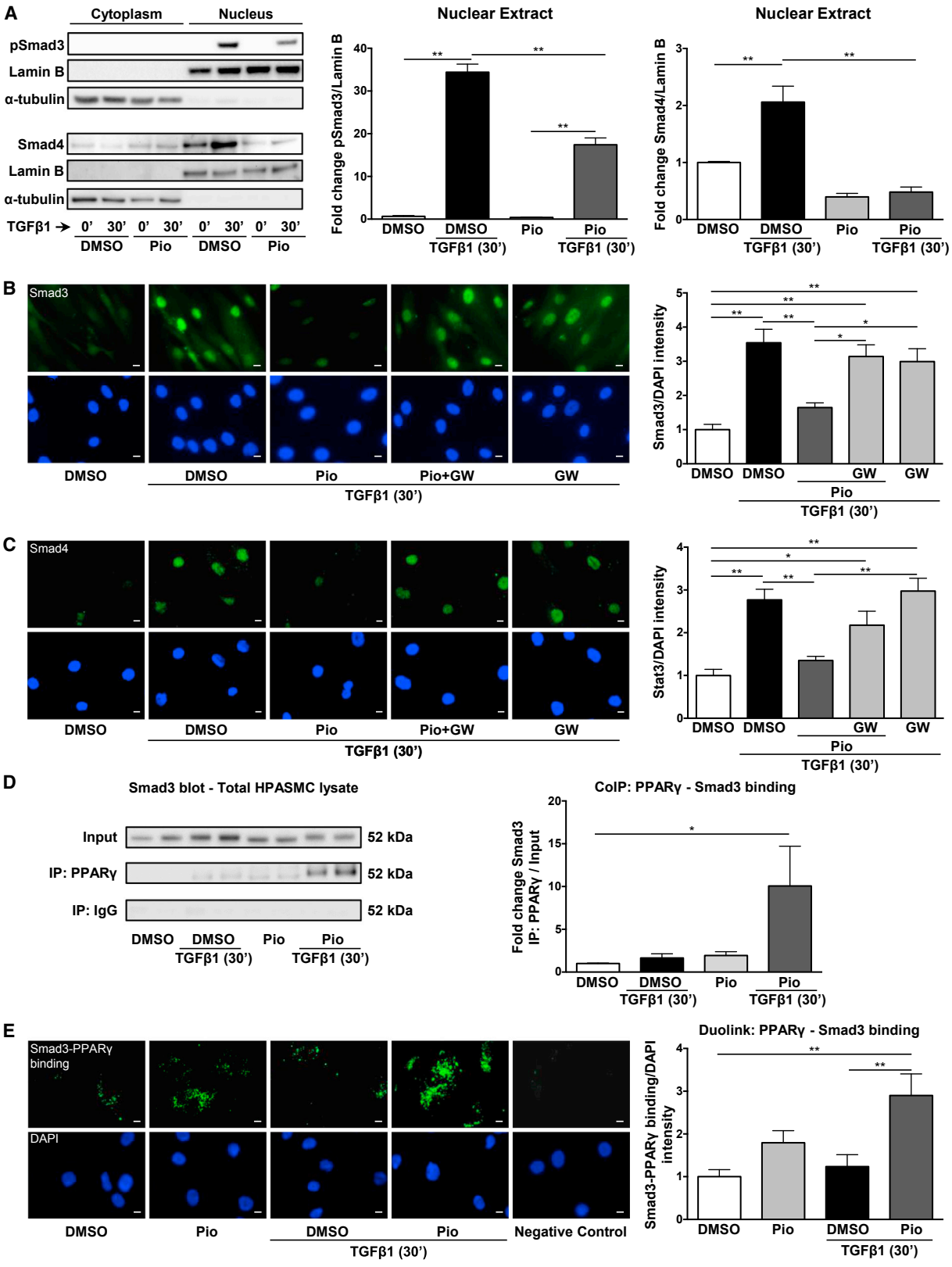

(legend on next page)

PPARγ Activation Inhibits the TGFβ1 Non-canonical Phosphorylation Cascade Stat3/FoxO1

In contrast to canonical signaling, TGFβ1 non-canonical pathways are hardly known, particularly in PAH. Since previous studies emphasize the role of pro-inflammatory Stat3 (Malenfant et al., 2013; Meloche et al., 2013; Paulin et al., 2011) and vasoprotective, dephosphorylated nuclear FoxO1 (Savai et al., 2014) in VSMC proliferation and PAH, we hypothesized that both factors could be regulated by TGFβ1.

TGFβ1 induced a 2.5-fold increase in pStat3 and pFoxO1 at 10 min in total cell lysate (Figure 3A). Moreover, TGFβ1 induced rapid translocation of pStat3 into the nucleus (Figures 3B and 3C) that was accompanied by nuclear exit of pFoxO1 to the cytoplasm, where it is known to be inactive (Savai et al., 2014) (Figures 3B and 3D). Pioglitazone strongly inhibited TGFβ1-induced phosphorylation and shuttling of both Stat3 (Figures 3B and 3C) and FoxO1 (Figures 3B and 3D).

To investigate this inhibition further, we tested for direct binding of PPARγ to Stat3 or FoxO1. CoIP demonstrated that PPARγ (activated by pioglitazone) immunoprecipitated with Stat3 in the presence of TGFβ1 (Figure 3F). To identify where this interaction occurs, we performed coIP on cytoplasmic and nuclear fractions. After pre-incubation with pioglitazone and TGFβ1 stimulation, activated PPARγ bound to pStat3 and total Stat3 in the nucleus (Figure 3G). We did not observe any direct physical interaction between PPARγ and FoxO1 (data not shown), although activated PPARγ inhibited FoxO1 phosphorylation and shuttling (Figures 3A and 3B). Therefore, we hypothesized that FoxO1 is phosphorylated through—and thus downstream of—pStat3. To address this question, we stimulated HPASMCs with TGFβ1 in the presence of the Stat3 inhibitor BP-1-102, which selectively binds to the Stat3 SH2 domain and blocks Stat3 phosphorylation, without any effect on other kinases. In HPASMCs pre-incubated with Stat3 inhibitor, TGFβ1 failed to induce FoxO1 phosphorylation and inactivation (Figures 3E and S3B), indicating that TGFβ1 induces FoxO1 inactivation through pStat3. Taken together, these results reveal a non-canonical TGFβ1-Stat3-FoxO1 axis in VSMCs: TGFβ1 induces Stat3 phosphorylation and nuclear shuttling, where it promotes phosphorylation (inactivation) of FoxO1. Activated PPARγ binds to pStat3 and Stat3 in the nucleus, decreases pStat3 accumulation in the nucleus, and overall decreases nuclear Stat3, thus blocking the TGFβ1-Stat3-FoxO1 pathway.

BMP2-Induced PPARγ Directly Binds to Genes that Are Relevant to VSMC Proliferation and Metabolism, such as PFKP

Besides antagonistic functions between BMP2-PPARγ and TGFβ1-Stat3-FoxO1, we further hypothesized that PPARγ could directly regulate genes relevant for VSMC proliferation, energy metabolism/mitochondrial activity, and other key cellular functions. For this purpose, we screened PPARγ target genes using chromatin immunoprecipitation with a PPARγ antibody, followed by deep sequencing (ChIP-DNA-seq) in negative control and PPARγ knockdown HPASMCs stimulated with BMP2. Figure 4A presents the list of the first 50 targets sorted by decreasing enrichment in the short hairpin RNA (shRNA) negative control cells stimulated with BMP2. We found that PPARγ particularly bound to nine target genes (TBC1D32, MIR125B2, PMAIP1, MIR3120, CCNG1, RPRM, NOL7, ZRANB3, and CEP192) related to cell cycle, proliferation, and apoptosis; two targets (ATP5G3 and PFKP) related to energy metabolism; three targets (DCLK2, HAPLN1, and MYOZ1) related to cellular cytoskeleton and extracellular matrix; and four targets (NR2F2, CILP, CTSC, and HTR1B) interacting with TGFβ (Figures 4A and S4A; Table S1). Overall, the ChIP-seq screening revealed that activated PPARγ interacts directly with pathways regulating HPASMC proliferation and metabolism and, as such, besides direct TGFβ1 pathway inhibition (Figures 1, 2, and 3), can counteract TGFβ1 function.

To further demonstrate the opposing roles of TGFβ1 and PPARγ in energy metabolism, we studied PFKP—a PPARγ target gene we identified by ChIP-seq (Figure 4A). PFKP is a rate-limiting enzyme in glycolysis, catalyzing the conversion of fructose 6-phosphate to fructose 1,6-bisphosphate, allowing oxidative phosphorylation. In line with our mitochondrial respiration/oxidative phosphorylation (OXPHOS) data (Figures 1E and 1F), PPARγ activation by pioglitazone decreased PFKP at baseline and abolished its induction by TGFβ1 in HPASMCs (Figure 4C). In addition to the known regulation of glycolysis, recombinant PFKP induced HPASMC proliferation in culture (cell count, Figure 4D; MTT, Figure S5A).

PFKP Protein Expression Is Enhanced in Small-to-Medium-Sized Pulmonary Arteries of Human PAH Lungs, and in Cultured PAH PASMCs Stimulated with TGFβ1

To determine the relevance of PFKP in human PAH, PFKP expression was analyzed by immunohistochemistry in pulmonary arteries from idiopathic PAH (IPAH) patients and control subjects (downsizing donor lungs). PFKP staining was much stronger in the media and the adventitia of pulmonary arteries and arterioles from IPAH patients than controls (Figure 4E). Of note, the main large arteries from both PAH and control lungs had a faint PFKP staining compared to small and medium arteries (Figure S5B). The higher PFKP expression in PAH versus controls was confirmed by western blot in explanted HPASMCs

Figure 2. The PPARγ Agonist Pioglitazone Inhibits TGFβ1-Induced Phosphorylation and Shuttling of Smad3 and Smad4 in HPASMCs

(A–E) To explore the canonical TGFβ1 signaling, HPASMCs were starved for 24 hr, pre-incubated with the PPARγ agonist pioglitazone (10 μM) or DMSO (equivalent) for another 24 hr, and stimulated with TGFβ1 (5 ng/mL) for 30 min.

(A) pSmad3 and Smad4 protein expression in cytoplasmic and nuclear extracts was measured by western blot (n = 3 experiments).

(B and C) In immunofluorescence experiments, the adherent cells were stained for total Smad3 (B) or Smad4 (C) (green) and DAPI (nuclear DNA; in blue). Representative immunofluorescence pictures are shown (scale bar, 40 μm). The histogram represents the quantification of the ratio of Smad3 (B) or Smad4 (C) over DAPI intensity (n = 3 experiments).

(D and E) To understand PPARγ interaction with Smad3, coIP on total cell lysate (D) and Duolink assay (E) were performed.

(D) Total cell lysate were subjected to coIP with anti-PPARγ or IgG antibodies and immunoblotted for Smad3 (n = 2 experiments).

(E) Representative pictures for Duolink assay are shown (scale bar, 40 μm), and quantification was performed on random pictures (n = 2 experiments).

All values are expressed as mean ± SEM; *p < 0.05; **p < 0.01.

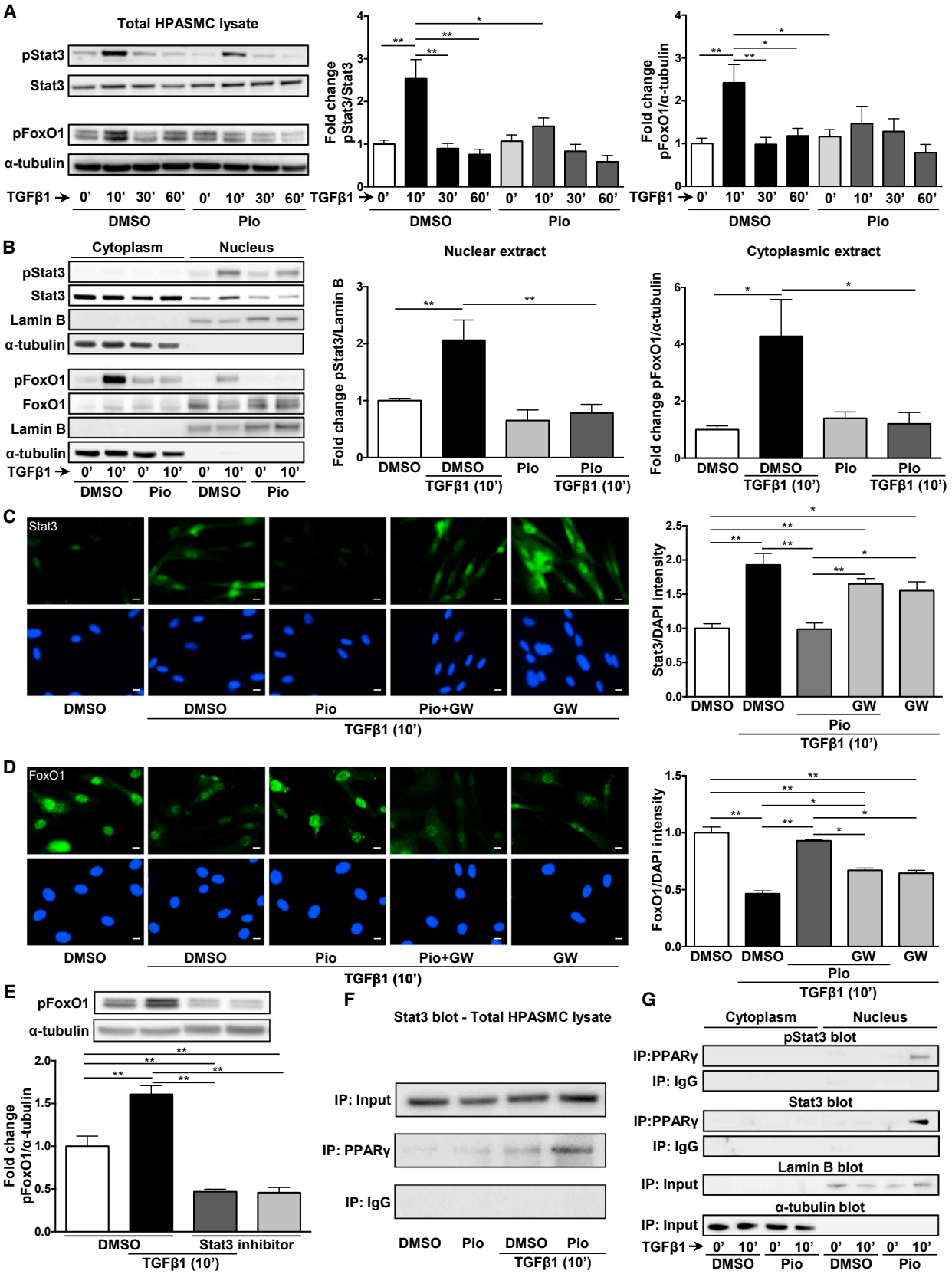

(legend on next page)

from PAH versus COPD patients: recombinant TGFβ1 induced stronger PFKP expression in PAH than COPD HPASMCs in vitro and this induction was inhibited by pioglitazone (Figure 4F). Our results show that PAH HPASMCs are more sensitive to TGFβ1-induced PFKP expression, which can be inhibited by PPARγ activation.

TGFβ1-Induced Smad3 Directly Binds to Genes Relevant to VSMC Proliferation and Metabolism

Next, we screened Smad3 target genes by ChIP-DNA-seq in negative control and PPARγ-knockdown HPASMCs, stimulated with TGFβ1. We first hypothesized that HPASMCs with low PPARγ expression would have higher Smad3-DNA binding: indeed, at baseline we found 1,260 Smad3-DNA-binding peaks in negative control versus 3,979 in the PPARγ-knockdown group. We then selected the first 50 targets sorted by decreasing enrichment in the shRNA negative control cells stimulated with TGFβ1 (Figure 4B). We found that Smad3 particularly bound to one target (BRSK2) related to cell cycle, proliferation, and apoptosis; four targets (PPP1R3G, AACS, ANO5, and AQP1) related to energy metabolism; four targets (COL23A1, EMB, GJB6, and SPON1) related to cytoskeleton, cell-cell adhesion, and extracellular matrix; and three targets (NR1H4, PRMT6, and ATF7IP2) related to transcription factors (Figures 4B and S4B; Table S2). Of note, among all target genes, we have not found BMP2, BMPR2, or PPARγ. Our ChIP-seq screening reveals that activated Smad3 interacts directly with pathways regulating HPASMC proliferation; energy metabolism; and cytoskeleton, cell-cell adhesion, and extracellular matrix.

To further investigate the antagonistic roles of TGFβ1/Smad3 and PPARγ, we studied expression of PPP1R3G—a Smad3 target gene we identified by ChIP-seq (Figure 4B). PPP1R3G is a regulatory subunit of protein phosphatase 1 and promotes glycogen synthase activity, thus increasing glycogenesis in hepatocytes (Zhang et al., 2014). Interestingly, TGFβ1 decreased PPP1R3G protein expression in HPASMCs, which was reversed by pioglitazone (Figure 4C).

The BMP2-PPARγ Axis Inhibits Expression of TGFβ1 Downstream Targets

We investigated whether PPARγ activation inhibits TGFβ1-induced target expression. In HPASMCs, TGFβ1 stimulation decreased mRNA expression of PPARγ (Figures 5A and 6A) and increased mRNA expression of TGFBR1 (Figures 5A and 6A), connective tissue growth factor (CTGF; Figures 5A and 6A), α-smooth muscle actin (ACTA2; Figures 5A and 6A), and TGFβ1 (Figure 5A); these expression changes were inhibited by pioglitazone (Figure 5A).

To elucidate whether PPARγ is required for BMP2 to inhibit TGFβ1-induced target gene expression, we applied stable knockdown of PPARγ in HPASMCs. After BMP2 pre-incubation, TGFβ1 failed to significantly induce the above-described mRNA changes of PPARγ, TGFBR1, CTGF, and ACTA2 expression in negative control, but not in shRNA PPARγ knockdown HPASMCs (Figure 6A). These data support the antagonistic role of BMP2 on TGFβ1 target expression and the central role for PPARγ, linking these two pathways.

TGFβ1 Inhibits PPARγ Expression through miR-130a

We next sought to understand how TGFβ1 decreases PPARγ in HPASMCs. TGFβ1 rapidly (6 hr) induced the miR-130a/301b cluster (Figure 5B). Interestingly, based on a bioinformatics database (Targetscan), miR-130a is predicted to target PPARγ mRNA (Figure 5C). Therefore, we reasoned that TGFβ1 rapidly decreases PPARγ mRNA through induction of miR-130a. Indeed, we found that pre-miR-130a transient transfection decreased PPARγ mRNA level but also increased mRNA expression of TGFβ1, TGFBR1, and their downstream targets CTGF and ACTA2 (Figure 5D). To confirm the functional role of miR-130a in TGFβ1-induced downregulation of PPARγ, we next knocked down miR-130a in HPASMCs by antagomiR transfection. Shortly after TGFβ1 stimulation (3–6 hr) in negative control cells, we found that PPARγ mRNA expression went down as miR-130a went up in control cells (Figure 5E). Importantly, in cells treated with antagomiR-130a, TGFβ1 failed to decrease PPARγ mRNA at 6 hr (Figure 5E). Hence, our findings demonstrate that TGFβ1 rapidly decreases PPARγ mRNA via the miR-130a/301b cluster in HPASMCs.

Expression of the miR-130a/301b Cluster Downstream of TGFβ1 Is Increased in Pulmonary Arteries of PAH Patients

To explore whether the miR-103a/301b cluster that we had found to be downstream of TGFβ1 in cultured HPASMCs (Figure 5B) is highly expressed in human PAH lungs, we determined the vascular miR-103a/301b expression by qPCR in laser microdissected pulmonary arteries from IPAH patients and control subjects (downsizing donor lungs). Indeed, expression of miR-130a and miR-301b was increased 1.5-fold and 2.5-fold in

Figure 3. The PPARγ Agonist Pioglitazone Inhibits TGFβ1-Induced Phosphorylation and Shuttling of Stat3 in the Nucleus and FoxO1 in the Cytoplasm in HPASMCs

(A–D, F, and G) To explore non-canonical TGFβ1 signaling, HPASMCs were serum starved for 24 hr, pre-incubated with the PPARγ agonist pioglitazone (10 μM) or DMSO (volume equivalent) for another 24 hr, and stimulated with TGFβ1 (5 ng/mL) for 10, 30, or 60 min as mentioned.

(A) The time response for phosphorylation of Stat3 (Tyr705) and FoxO1 (Thr24) in total cell lysate was quantified by western blot (n = 3 experiments).

(B) Levels of pStat3, Stat3, pFoxO1, and FoxO1 protein in the cytoplasmic and nuclear extracts were quantified by western blot (n = 3 experiments).

(C and D) For immunofluorescence, the cells were stained for total Stat3 (C) or FoxO1 (D) (green) and DAPI (nuclear DNA; in blue). Representative pictures are shown (scale bar, 40 μm). The histogram represents the quantification of the ratio of Stat3 (C) or FoxO1 (D) over DAPI intensity (n = 3 experiments).

(E) The link between Stat3 and FoxO1 was clarified using the Stat3 inhibitor (BP-1-102). After 24 hr of serum starvation, HPASMCs were pre-incubated with BP-1-102 (10 μM) or DMSO (equivalent) for 1 hr and stimulated with TGFβ1 (5 ng/mL) for 10 min. The level of pFoxO1 protein expression in total cell lysates was measured by western blot and densitometry (n = 3 experiments).

(F and G) To assess PPARγ interaction with Stat3, coIP on total cell lysate (F) and cytoplasmic and nuclear extracts (G) was performed. Samples were subjected to coIP with anti-PPARγ or IgG antibodies and immunoblotted for pStat3 or Stat3 (n = 2 experiments).

All values are expressed as mean ± SEM; *p < 0.05; **p < 0.01.

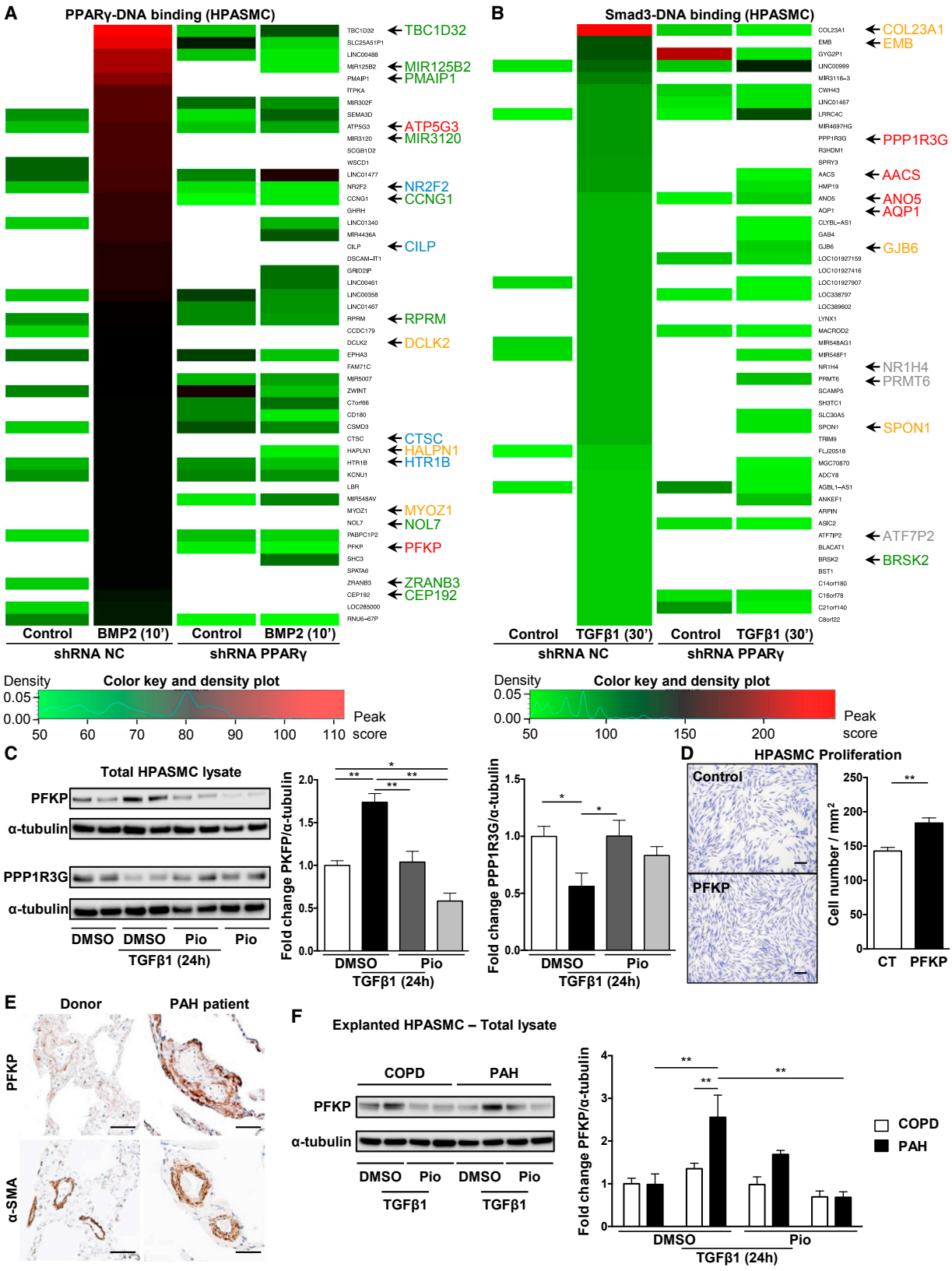

(legend on next page)

pulmonary arteries (inner diameter < 500 μm) of IPAH patients versus controls, respectively (Figure 5F).

The BMP2-PPARγ Axis Inhibits PFKP through Induction of miR-331-5p

To identify miRNAs downstream of the BMP2/BMPR2-PPARγ axis, we have screened miRNA expression using TaqMan Human MicroRNA Arrays (cards A and B, Life Technologies) in shRNA PPARγ knockdown and control HPASMCs, pre-incubated with BMP2, and stimulated with TGFβ1 (data not shown). By doing so, we discovered—and further validated by single qPCR—that miR-331-5p (Figure 5G) and miR-148a (Figure S5D) were induced by BMP2 in shRNA negative control HPASMCs, but not in PPARγ knockdown HPASMCs. This result suggests that BMP2-induced miR-148a and miR-331-5p expression is mediated by PPARγ. Intriguingly, miR-148a is known to repress cell proliferation in bladder cancer cells (Wang et al., 2016), and miR-331-5p is predicted to target PFKP mRNA (Targetscan; Figure 5H). Consistently, transfection of HPASMCs with pre-miR-331-5p decreased PFKP mRNA (Figure 5I) and protein (Figure S5E) expression. Thus, our results indicate that BMP2-BMPR2-PPARγ signaling in VSMCs inhibits the pro-proliferative metabolic regulator PFKP through induction of miR-331-5p.

PPARγ Disruption in VSMCs, In Vitro or In Vivo, Leads to Increased TGFβ1 Signaling

To explore the key role of PPARγ as gatekeeper between TGFβ1 and BMP2 pathways, we disrupted PPARγ in VSMCs. First in vitro (HPASMCs), we observed that decreased PPARγ expression (lentiviral shRNAi) led to increased mRNA expression of TGFβ1 and its targets CTGF and ACTA2 (Figure 6B). Next, we used a mouse with targeted deletion of PPARγ in SMCs (*SM22α Cre PPARγ$^{flox/flox}$* mouse model, or SMC *PPARγ$^{-/-}$* mice) that we had previously shown to develop PAH and pulmonary artery remodeling (Hansmann et al., 2008). Consistent with our overall hypothesis, we found mRNA expression of TGFβ1, CTGF, and ACTA2 to be increased in total lungs of SMC *PPARγ$^{-/-}$* versus littermate control mice (Figure 6C). Immunohistochemistry for CTGF (Figure 6D) and αSMA (Figure 6E) on lung sections revealed that CTGF and αSMA protein expression was higher in the media of SMC *PPARγ$^{-/-}$* versus littermate control mice. Overall, these results illustrate the key role of PPARγ (downstream of BMPR2) to equilibrate TGFβ1 signaling in PASMCs.

TGFβ1-Overexpressing Mice Develop PAH that Is Fully Reversed by PPARγ Activation

Although emerging evidence indicates that TGFβ1 is elevated in plasma from PAH patients, it is unknown whether TGFβ1 itself triggers PAH. To address this question, we studied for the first time a transgenic TGFβ1 (TG-TGFβ1) mouse model with heightened circulating TGFβ1 for evidence of PAH (see STAR Methods and Figure S6). Control and transgenic male mice were divided into two sets: a first set of 10- to 12-week-old animals, and a second set untreated or orally treated with the PPARγ agonist pioglitazone for 5 weeks, and sacrificed at 15–17 weeks of age. We found both 10- to 12-week-old and 15- to 17-week-old TG-TGFβ1 mice to have PAH in room air, as judged by elevated RV systolic pressure (RVSP; Figures 7A and S6D) and RV mass (RV/body weight ratio; Figure 7B) versus controls. Intriguingly, 5 week pioglitazone treatment fully reversed PAH and RVH. At 15–17 weeks, TG-TGFβ1 mice, compared to controls, had higher media thickness index (Table S3; representative lung αSMA staining in Figure 7F), indicating heightened peripheral pulmonary artery muscularization and loss of small vessels by 39% (outer diameter < 50 μm, $p < 0.01$; Figure 7C; representative vWF staining pictures in Figure S7A), both inhibited by pioglitazone. In addition, TG-TGFβ1 mice had a higher degree of SMC proliferation and fibrosis in the pulmonary arteries, as judged by positive proliferating cell nuclear antigen (PCNA) and collagen (Masson's trichrome) artery staining, a vascular phenotype that was absent in TG-TGFβ1 mice treated with pioglitazone (Figure S7A).

We next sought to understand how PPARγ activation reverses the PAH phenotype in TG-TGFβ1 mice. Consistent with our previous findings in cultured HPASMCs, SMC *PPARγ$^{-/-}$* mice, and human PAH samples, mRNA expression of TGFβ1 and CTGF was heightened in the main pulmonary artery of TG-TGFβ1 mice (Figure 7D), as was expression of CTGF and ACTA2 in total lung of TGFβ1-overexpressing mice (Figures S7C and S7E). Accordingly, the protein level of TGFβ1, CTGF, αSMA (synonym, ACTA2), and PFKP was increased in total lung of TG-TGFβ1 mice (Figures 7G and S7D). Moreover, CTGF (Figure S7A) and αSMA (Figure 7F) protein expression was elevated in the pulmonary arteries as

Figure 4. ChIP-Seq Reveals BMP2 and TGFβ1 Downstream Targets by Means of PPARγ- or Smad3-DNA Binding, and Its Dependency on PPARγ Expression, in HPASMCs

HPASMCs were transduced using lentivirus constructs with shRNA negative control (NC) or small hairpin sequences targeting PPARγ mRNA (shRNA).

(A and B) For ChIP-seq, transduced HPASMCs were serum starved and stimulated with BMP2 (10 min, 10 ng/mL) or TGFβ1 (30 min, 5 ng/mL) (n = 3 experiments). The heatmaps represent a selection of the first 50 targets sorted by decreased enrichment in the shRNA NC cells stimulated with BMP2 (BMP-induced PPARγ-DNA binding; A) or TGFβ1 (TGFβ1-induced Smad3-DNA binding; B) (green to red reflects low-to-high DNA binding). In these selections, PPARγ (A) and Smad3 (B) targets were highlighted and grouped by function: in green, cell cycle, proliferation, and apoptosis; in red, energy metabolism; in orange, cytoskeleton, cell-cell adhesion, and extracellular matrix; in blue, targets interacting with TGFβ; and in gray, transcription factors.

(C) HPASMCs were starved 24 hr, pre-incubated with the PPARγ agonist pioglitazone (10 μM) or DMSO (equivalent) for another 24 hr, and stimulated with TGFβ1 (5 ng/mL) for 24 hr. The expression of PKFP and PPP1R3G in total cell lysate was quantified by western blot and combines three independent experiments.

(D) HPASMCs were serum starved for 48 hr and stimulated with recombinant PFKP protein (100 ng/mL) for 72 hr. Cell proliferation was assessed by cell count on fixed cells stained with crystal violet. Data are representative of twelve replicates in each of two independent experiments.

(E) Human lung serial sections were analyzed by immunohistochemistry for PFKP expression in the pulmonary arteries of four IPAH patients and three healthy donors. Representative PFKP staining is shown together with αSMA staining in the same arteries (scale bar, 50 μm).

(F) HPASMCs isolated from pulmonary arteries of COPD (control, n = 3) or PAH patients (n = 3). The cells were starved for 24 hr and pre-incubated with pioglitazone (10 μM) or DMSO (equivalent) for another 24 hr and then stimulated with TGFβ1 (5 ng/mL) for 24 hr.

All values are expressed as mean ± SEM; *$p < 0.05$; **$p < 0.01$.

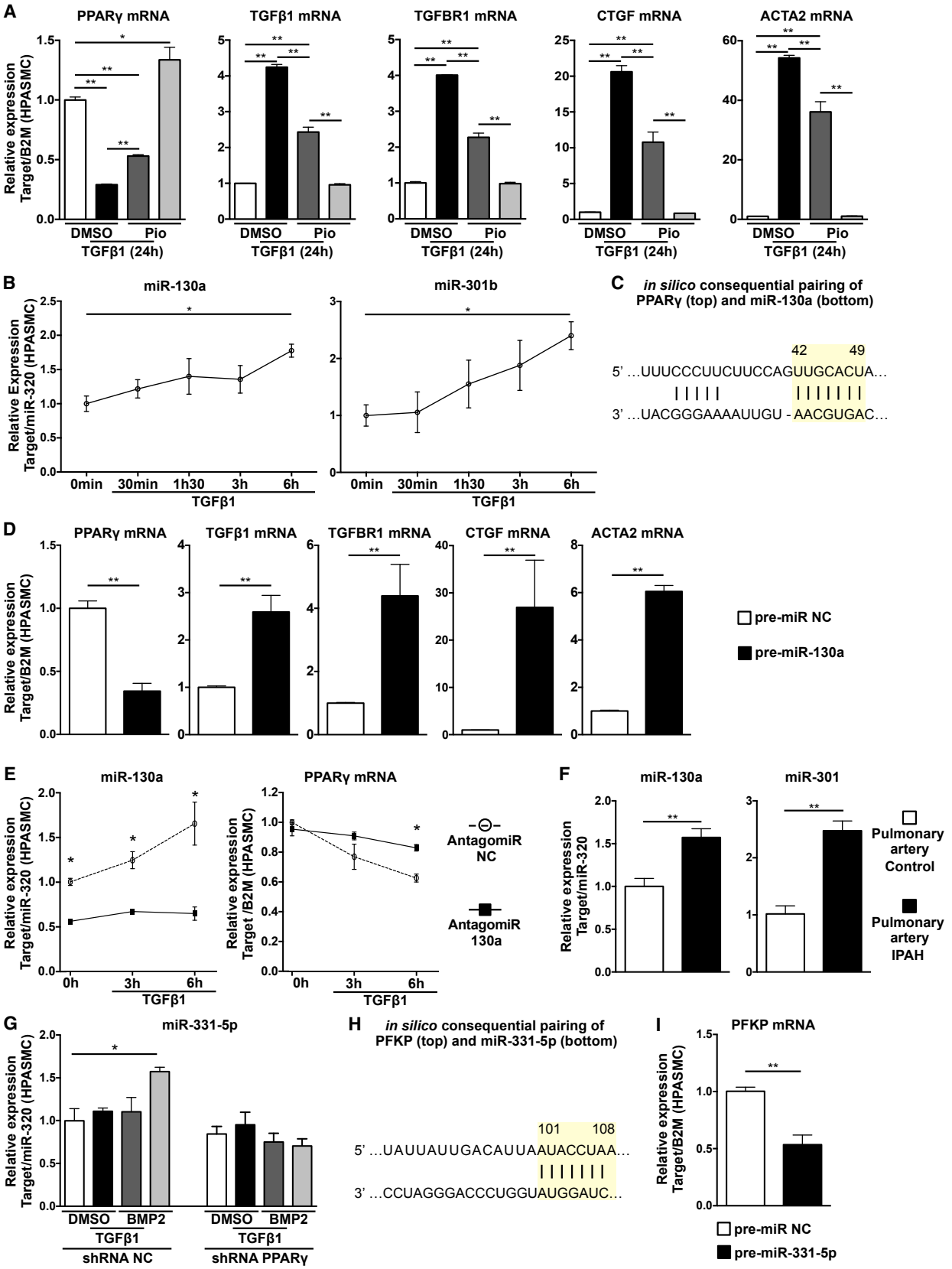

(legend on next page)

demonstrated by immunohistochemistry. The induction of these TGFβ1 targets in the lung and pulmonary arteries of the TG-TGFβ1 mice was inhibited by pioglitazone treatment (Figures S7D and S7E). The expression of the miR-130a/301b cluster was also increased in the main pulmonary artery of TG-TGFβ1 mice and inhibited by pioglitazone treatment (Figure 7E). We have shown in PAH patients versus controls that PFKP expression was heightened in the small pulmonary arteries only (inner diameter < 200 μm; Figure S5B). Accordingly, PFKP mRNA (Figure 7D) and its regulator miR-331-5p (Figure 7E) were unaffected in the main pulmonary artery of TG-TGFβ1 mice, but PFKP protein was found elevated in total lung lysates of TG-TGFβ1 and inhibited by pioglitazone. Finally, both canonical (pSmad3) and non-canonical (pStat3-pFoxO1) TGFβ1 pathways were activated in the lungs of TG-TGFβ1 mice and completely blocked by pioglitazone treatment (Figure 7H). In summary, our in vivo studies introduce a normoxic PAH mouse model and suggest that the PPARγ agonist pioglitazone can counteract TGFβ1 signaling, both the canonical Smad3 and the non-canonical Stat3-FoxO1 pathway, thereby fully reversing PAH, RVH, and vascular remodeling.

DISCUSSION

In this study, we identified a non-canonical, pro-proliferative TGFβ1-Stat3-FoxO1 axis in VSMCs (Figure S1). TGFβ1 induced Stat3 phosphorylation and shuttling into the nucleus, where it promoted FoxO1 phosphorylation and pFoxO1 exit to the cytoplasm, thus preventing FoxO1-chromatin binding (Hatta and Cirillo, 2007) and proper regulation of energy metabolism and proliferation. Interestingly, we observed in HPASMCs that TGFβ1 decreased PPARγ mRNA expression by inducing miR-130a—a known suppressor of PPARγ mRNA (Bertero et al., 2014)—which we found to be significantly increased in pulmonary arteries of PAH patients. On the other hand, we found that activated PPARγ inhibited both canonical TGFβ1-pSmad3/4 and non-canonical TGFβ1-Stat3-FoxO1 signaling in VSMCs through physical interactions with Smad3 and Stat3. In addition, ChIP-seq in HPASMCs revealed that BMP2-induced PPARγ and TGFβ1-induced Smad3 bind to proliferation- and metabolism-related genes (e.g., PFKP and PPP1R3G), whereas PPARγ and Smad3 did not directly interact with TGFβ1/TGFBR and BMP2/BMPR, respectively. Accordingly, PPARγ activation by BMP2 or pioglitazone inhibited TGFβ1-induced mitochondrial activation (respiration) and HPASMC proliferation. In addition, PFKP protein expression was increased in PASMCs from pulmonary arteries of PAH patients, in vitro and in vivo, and PFKP induced HPASMC proliferation. Besides PPARγ binding to the PFKP gene (protein-DNA interaction), BMP2-PPARγ downregulated the pro-proliferative/pro-glycolytic key enzyme PFKP through induction of miR-331-5p. Consistent with these results, we found in a mouse model that heightened circulating TGFβ1 leads to spontaneous development of PAH, RVH, peripheral pulmonary artery muscularization, and small vessel loss in vivo. All of these PAH features were fully reversed by oral treatment with the PPARγ agonist pioglitazone.

We have previously shown that PPARγ is a downstream effector of anti-proliferative BMP2-BMPR2, and that PPARγ deletion in SMCs (Hansmann et al., 2008) or endothelial cells (Guignabert et al., 2009) results in PAH. We expand this work now on the mechanistic level by demonstrating that PPARγ disruption in PASMCs induced activation of TGFβ1 in vitro and in vivo (SMC *PPARγ*$^{-/-}$ mice). Others have also described enhanced TGFβ1 signaling with BMPR2 disruption in PASMCs (Morrell, 2006; Newman et al., 2008). Collectively, our results highlight the importance of the BMP2-PPARγ axis to balance detrimental TGFβ1 pathways in the vasculature.

Previously, indirect evidence suggested that TGFβ1 and the targets within its pathway (e.g., CTGF) are associated with the pathobiology of PAH (Li et al., 2016; Selimovic et al., 2009). We found that human explanted PAH PASMCs were more sensitive to mitogenic TGFβ1 stimulation than control cells (COPD PASMCs), resulting in more pronounced proliferation and higher expression of PFKP and CTGF. Our PAH mouse model of TGFβ1 overexpression (TG-TGFβ1) demonstrates that heightened circulating TGFβ1 induces a PAH phenotype characterized by peripheral pulmonary artery muscularization and small vessel loss. In the TG-TGFβ1 mouse pulmonary artery, and in HPASMC culture, we found that TGFβ1 not only induced target mRNA expression (PFKP, CTGF, and αSMA), but also rapidly initiates a phosphorylation cascade: the known canonical

Figure 5. TGFβ1 Inhibits PPARγ mRNA Expression via Induction of the miR-130a / 301b Cluster

(A) After 24 hr of serum starvation, HPASMCs were pre-incubated with pioglitazone (10 μM) or DMSO (equivalent) for another 24 hr and stimulated with TGFβ1 (5 ng/mL) for 24 hr. PPARγ and TGFβ1 pathway mRNA expression was analyzed by qPCR (n = 3 experiments).

(B) HPASMCs were serum starved for 48 hr and then stimulated with TGFβ1 (5 ng/mL) for 0–6 hr. The expression of miR-130a and miR-301b was measured by qPCR (n = 3 experiments).

(C) Predicted miR-130a - PPARγ mRNA binding based on the bioinformatics database Targetscan.

(D) HPASMCs were transfected with a pre-miRNA negative control (NC) or pre-miR-130a, serum starved for 24 hr, and harvested to evaluate mRNA levels (n = 3 experiments).

(E) To validate that TGFβ1 decreases PPARγ via miR-130a, HPASMCs were transduced with a negative control (NC) antagomiR or antagomiR directed against miR-130a; after 24 hr of serum starvation, the cells were stimulated for 3 or 6 hr with TGFβ1 (5 ng/mL). miR-130a and PPARγ mRNA expressions were measured by qPCR (n = 3 experiments).

(F) To explore whether the miR-103a/301b cluster is relevant in human PAH lungs, miRNA expression was analyzed by qPCR in laser microdissected pulmonary arteries (inner diameter < 500 μm) from IPAH patients (n = 5) and control subjects (downsizing donor lungs, n = 5).

(G) HPASMCs were transduced using lentivirus constructs with shRNA negative control (NC) or small hairpin sequences targeting PPARγ mRNA (shRNA). After 24 hr of serum starvation, HPASMCs were pre-incubated with BMP2 (10 ng/mL) for another 24 hr and stimulated with TGFβ1 (5 ng/mL) for 6 hr. miR-331-5p expression was measured by qPCR (n = 3 experiments).

(H) Predicted miR-331-5p - PFKP mRNA binding based on the bioinformatics database Targetscan.

(I) HPASMCs were transfected with a pre-miRNA negative control (NC) or pre-miR-331-5p, serum starved for 24 hr, and harvested to evaluate PFKP mRNA levels (n = 3 experiments).

All values are expressed as mean ± SEM; *p < 0.05; **p < 0.01.

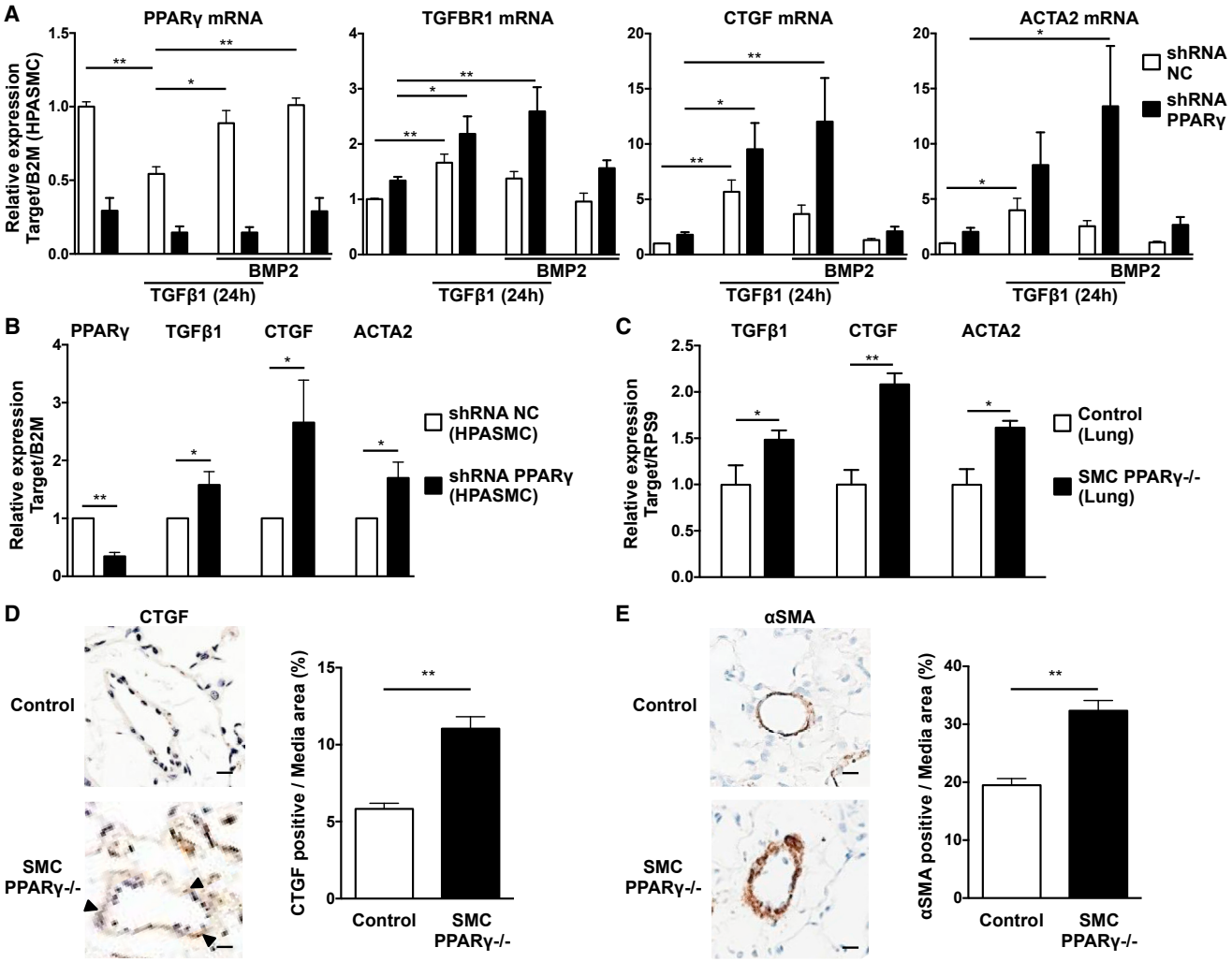

Figure 6. Knockdown of PPARγ in SMCs In Vitro, or Targeted Deletion of PPARγ in SMCs In Vivo, Leads to Increased TGFβ1 Signaling

HPASMCs were transduced using lentivirus constructs with shRNA negative control (NC) or targeting PPARγ mRNA. Serum-starved HPASMCs were pre-incubated with BMP2 (10 ng/mL) for 24 hr and stimulated with TGFβ1 (5 ng/mL) for 24 hr.

(A) The mRNA expression of PPARγ, TGFβ1, CTGF, and ACTA2 was measured by qPCR (n = 3 experiments). Statistical analysis was done separately for shRNA NC and shRNA PPARγ.

(B) Transduced cells were starved for 48 hr and harvested to measure the mRNA expression by qPCR (n = 3 experiments).

(C–E) Lungs from mice with targeted deletion of PPARγ in SMCs (SM22α Cre PPARγ$^{flox/flox}$), and control mice, were used.

(C) mRNA expression was measured in total lung tissue by qPCR.

(D and E) Immunohistochemistry on lungs was performed for CTGF (D) and ACTA2 (E). The ratio of the positive area (dark brown stain) in the media of vessels to the media area was measured as a surrogate for specific protein expression level in the pulmonary vessels. Representative pictures are shown (scale bar, 10 μm); the arrows point to positive CTGF staining in the media. n = 4–7 animal per group.

All values are expressed as mean ± SEM; *p < 0.05; **p < 0.01.

pSmad3/Smad4 and the non-canonical pStat3-pFoxO1. Several groups reported on the importance of pro-inflammatory IL-6-Stat3 (Steiner et al., 2009), RAGE-Stat3-BMPR2-PPARγ (Meloche et al., 2013), and IL-6-Stat3-miR-17/92-BMPR2 (Brock et al., 2009) signaling loops for pulmonary artery muscularization and PAH development. In contrast, nuclear FoxO1 is a key factor for VSMC homeostasis and PAH prevention (Savai et al., 2014). To the best of our knowledge, ours is the first report on a pro-proliferative TGFβ1-Stat3-FoxO1 axis in VSMCs and its inhibition by PPARγ activation. Finally, we and others (Subramanian et al., 2012) found in PASMCs that TGFβ1 (24 hr) decreased PPARγ expression. In our study, TGFβ1 stimulation did not only decrease PPARγ mRNA synthesis (24 hr) but also rapidly suppressed PPARγ mRNA via induction of miR-130a (at 3–6 hr). Importantly, miR-130a/301b is a relevant cluster in human PAH since we quantified for the first time the increased pulmonary arterial miR-130a/301b expression in human IPAH lungs by laser capture microdissection.

Conversely, we delineated how BMP2-PPARγ inhibits TGFβ1 signaling and function, equilibrating the balance between these two pathways. In the TGFβ1-overexpressing PAH mouse model, the PPARγ agonist pioglitazone reversed RV systolic pressure

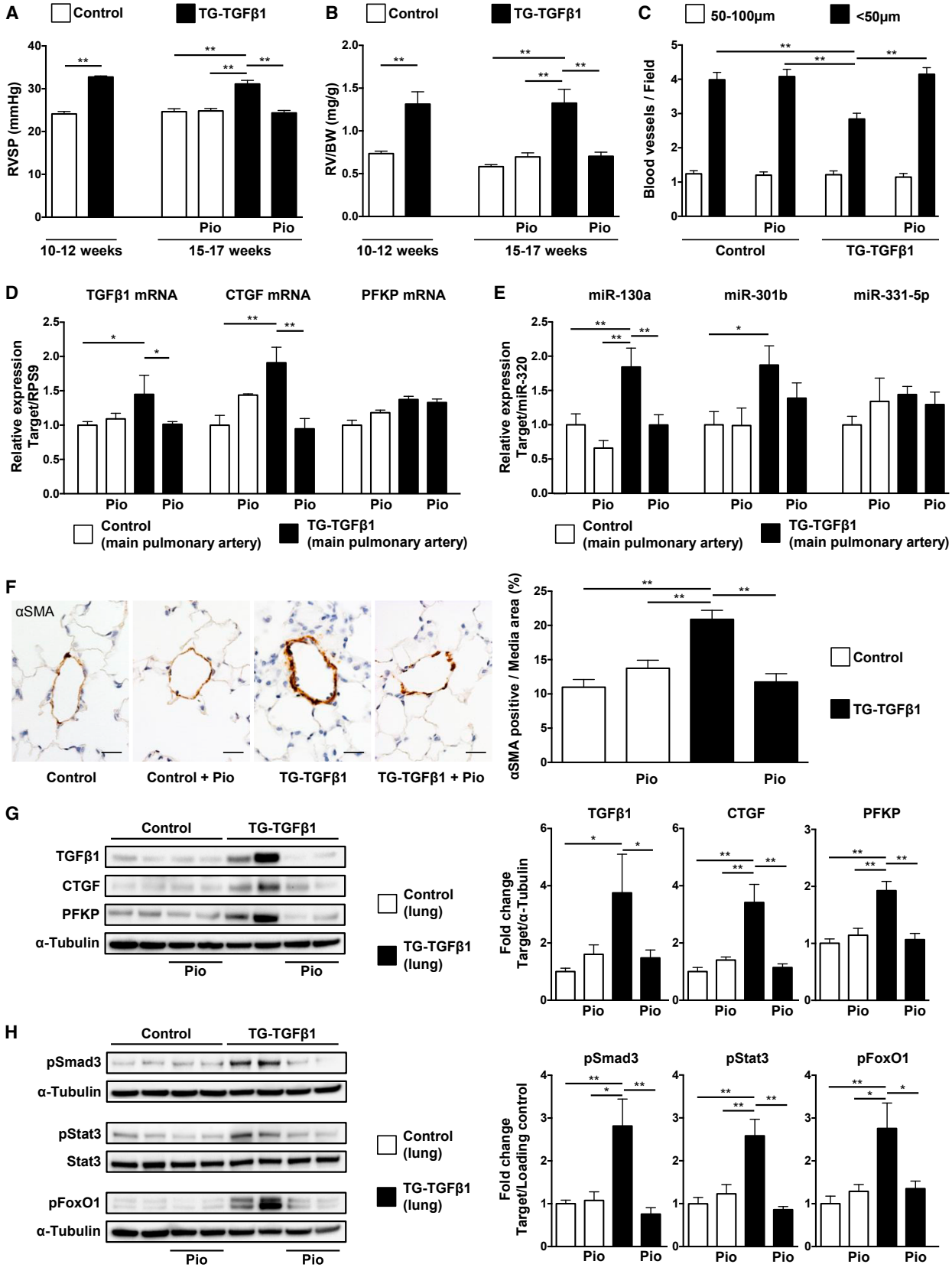

(legend on next page)

elevation and RVH and inhibited peripheral pulmonary artery muscularization and small vessel loss. Pioglitazone also counteracted TGFβ1-induced HPASMC proliferation and energy metabolism. BMPR2 was shown to preserve mitochondrial function in pulmonary artery endothelial cells by sustaining mitochondrial membrane potential (Diebold et al., 2015). Here, we demonstrate in VSMCs that PPARγ activation normalizes mitochondrial membrane potential and respiration (OXPHOS), counteracting TGFβ1. We also found that PFKP, a rate-limiting key enzyme promoting glycolysis and subsequent mitochondrial activity (OXPHOS), was upregulated by TGFβ1 and downregulated by PPARγ. On the other hand, expression of PPP1R3G, a crucial regulator of glycogen synthase activity and a promoter of glycogenesis, was decreased by TGFβ1, an effect that was inhibited by PPARγ activation. We propose that TGFβ1 drives glycolysis and inhibits glycogenesis in VSMCs, while BMP2-PPARγ act as functional antagonists of TGFβ1. Interestingly, TGFβ1 signaling regulates glucose tolerance and energy homeostasis, suggesting that blockade of the TGFβ1 pathway may be used for therapy of obesity and diabetes (Yadav et al., 2011). We link here glucose metabolism and cell proliferation by showing that the TGFβ1 downstream target PFKP induces VSMC proliferation, in addition to glycolysis regulation. PFKP is a new player relevant to human PAH, as we revealed increased PFKB expression in PASMCs from pulmonary arteries of PAH patients, in vitro and in vivo.

In addition to growth inhibition, PPARγ activation inhibited TGFβ1 target gene expression in murine pulmonary arteries and cultured HPASMCs. At the molecular level, pioglitazone inhibited phosphorylation and shuttling of Smad3/Smad4 and Stat3/FoxO1 through direct interaction between PPARγ-Smad3 (mainly in the cytoplasm) and PPARγ-Stat3 (in the nucleus). In line with our results, rosiglitazone inhibited TGFβ1-induced Smad3 phosphorylation in human aortic SMCs (Boucher et al., 2007). In human lung cancer (Lin et al., 2011), PPARγ binding to Smad3, but not to Smad4, has been reported. Pioglitazone inhibited interleukin-1β-induced Stat3 phosphorylation in rat VSMCs (Takata et al., 2002), and the PPARγ ligand 15-d-PGJ2 enhanced interaction between PPARγ and IL-6-activated Stat3 in a multiple myeloma cell line (Wang et al., 2004).

Taken together, our work identified PPARγ as major gatekeeper that regulates the complex balance between TGFβ1 and BMP2 pathways, thereby inhibiting metabolic and proliferative events downstream of TGFβ1 in VSMCs, and reversing PAH. Our pre-clinical results support the rationale for future TGFβ1-inhibiting therapies in PAH. Importantly, two clinically used, effective PAH-targeting drugs, trepostinil (Falcetti et al., 2010) and sildenafil (Wang et al., 2013), were shown to inhibit PASMC proliferation through PPARγ activation. Because of its multiple beneficial effects, the PPARγ agonist pioglitazone may be a suitable agent to reverse advanced pulmonary hypertensive vascular disease (Hansmann and Zamanian, 2009). Pioglitazone is an insulin-sensitizing drug of the TZD class, and in some studies is associated with weight gain and fluid retention, reversible heart failure, bone fractures (especially in postmenopausal women), and possibly bladder cancer (Dormandy et al., 2009). However, pioglitazone underwent a recent revival due to its positive risk-benefit ratio, with a safety profile that compares favorably with rosiglitazone (Loke et al., 2011; Soccio et al., 2014). In addition, the RECORD trial and its re-adjudication led to the removal of certain restrictions for rosiglitazone by the FDA in 2013 (Soccio et al., 2014). In general, TZDs are not thought to cause cardiac dysfunction directly, but rather to exacerbate heart failure via fluid retention in susceptible patients, i.e., those with multiple systemic cardiovascular risk factors such as diabetes (Soccio et al., 2014). Nevertheless, the clinical effects of pioglitazone on the heart in the presence or absence of insulin resistance are not quite clear (Soccio et al., 2014), but have been partly addressed in a recent randomized controlled trial: in patients (≥40 years of age) without diabetes who had insulin resistance along with a recent history of ischemic stroke or transient ischemic attack, the risk of stroke or myocardial infarction was significantly lower among patients who received pioglitazone (N = 1,939) than among those who received placebo (N = 1,937, follow-up 4.8 years; hazard ratio [HR] 0.76; 95% confidence interval [CI] 0.62–0.93; p = 0.007) (Kernan et al., 2016). Importantly, there was no significant between-group difference in the number of patients with heart failure (74 versus 71; p = 0.80), or in the number of patients hospitalized for heart failure (51 and 42; p = 0.35). Incident bladder cancer occurred in twelve patients in the pioglitazone group and in eight in the placebo group (p = 0.37) (Kernan et al., 2016).

Therefore, it will be important to conduct a risk-benefit analysis for pioglitazone in PAH patients of all age groups, and those with or without insulin resistance, given that PAH is an aggressive condition with a mortality of 25%–50% within 5 years of

Figure 7. Pioglitazone Reverses PAH, Spontaneously Developed in TGFβ1-Overexpressing Mice

Males from mouse model (TG-TGFβ1; genotype C57Bl/6-TgAlb/TGFβ1) with heightened circulating TGFβ1 concentrations were divided into two sets.

(A and B) A first set of 10- to 12-week-old control and TG-TGFβ1 mice (n = 3–4).

(A and H) A second set of 10- to 12-week-old control and TG-TGFβ1 mice was treated for 5 weeks on regular chow versus chow with incorporated pioglitazone (20 mg/kg/day) and sacrificed at 15–17 weeks of age (n = 7–12).

(A) Invasive hemodynamic measurements were performed before (10–12 weeks old) and after (15–17 weeks old) oral pioglitazone treatment to assess the right systolic pressure (RVSP).

(B) The right ventricle over the body weight ratio (RV/BW) was also determined as a measure of RVH.

(C) In the 15- to 17-week-old mice, peripheral pulmonary vessel loss was evaluated in lungs stained for von Willebrand factor by counting the number per field (magnification 200×) of small (diameter < 50 μm) and medium-sized (diameter 50–100 μm) vessels.

(D, E, and G) mRNA (D) and miRNA (E) expression of TGFβ1 targets was evaluated by qPCR in the main pulmonary artery. In the total lung, protein (G) levels of TGFβ1 targets were quantified by western blot.

(F) Lungs sections were stained for αSMA and the positive area (dark brown) in the media of vessels over the media area was measured to evaluate the expression of αSMA in the vessels. Representative pictures are presented (scale bar, 20 μm).

(H) The canonical (Smad3) and non-canonical (Stat3/FoxO1) TGFβ1 phosphorylation cascades were evaluated by western blot in the total lung.

Values are expressed as mean ± SEM; *p < 0.05; **p < 0.01.

diagnosis, even when treated according to the guidelines (Galiè et al., 2016; Humbert et al., 2010). Thus, based on the recent preclinical and clinical findings (Falcetti et al., 2010; Hansmann and Rabinovitch, 2010; Hansmann and Zamanian, 2009; Matsa et al., 2016; Soccio et al., 2014), PPARγ represents a promising target for the treatment of PAH and other TGFβ1-related conditions, such as parenchymal lung disease (pulmonary fibrosis and bronchopulmonary dysplasia), Marfan's syndrome, and metabolic dysfunction.

STAR★METHODS

Detailed methods are provided in the online version of this paper and include the following:

- KEY RESOURCES TABLE
- CONTACT FOR REAGENT AND RESOURCE SHARING
- EXPERIMENTAL MODEL AND SUBJECT DETAILS
  - SM22α Cre PPARγ $^{flox/flox}$ mice (SMC PPARγ −/−)
  - Transgenic mice TG-TGFβ1 (C57Bl/6-TgAlb/TGF-β1) with systemic TGFβ1 overexpression
  - HPASMC isolation and culture
  - Cell stimulations
  - Human lung tissue samples
- METHOD DETAILS
  - Hemodynamic measurements
  - Tissue harvest and preparation
  - Lung histology / immunohistochemistry
  - Pulmonary vascular morphometry and quantification
  - Lentiviral small hairpin RNA interference (shRNAi) gene silencing (stable knockdown)
  - Transient transfection with pre-miR or antagomiR
  - Immunofluorescence
  - Cell Counts / Crystal violet staining and quantification
  - MTT assay (cell proliferation)
  - Mitochondrial respiration
  - Mitochondrial transmembrane potential
  - Nuclear / Cytoplasmic extraction
  - Co-Immunoprecipitation (CoIP)
  - Western blot
  - ELISA
  - RT-qPCR
  - Laser capture microdissection (LCM)
  - Chromatin immunoprecipitation (ChIP) and DNA sequencing
- QUANTIFICATION AND STATISTICAL ANALYSIS
- DATA AND SOFTWARE AVAILABILITY
  - Data Resources

SUPPLEMENTAL INFORMATION

Supplemental Information includes seven figures and three tables and can be found with this article online at http://dx.doi.org/10.1016/j.cmet.2017.03.011.

AUTHOR CONTRIBUTIONS

L.C. designed experiments, performed experiments and data analysis, and wrote the manuscript. P.C. conducted bioinformatic analysis of the ChIP-DNA-seq data and revised the manuscript for important intellectual content. E.L., N.H., P.B., and J.G. performed experiments and data analysis, and revised the manuscript for important intellectual content. D.J. provided human lung tissue, supervised the laser capture microdissection experiments, and revised the manuscript for important intellectual content. M.M.M. assisted in the in vivo experiments, performed experiments and data analysis, and revised the manuscript for important intellectual content. G.H. generated the hypotheses, developed the experimental design and concept of the study, performed pilot experiments, supervised further experiments and data analysis, generated funding, and wrote the manuscript.

ACKNOWLEDGMENTS

We thank Christiane Ritter for excellent technical assistance, Drs. Anna Forst-Ludwig and Mandy Bloch for advice on the ChIP assay, and Dr. Stefan Engeli for providing the Seahorse equipment. This work was supported by the German Research Foundation (Deutsche Forschungsgemeinschaft, DFG grant HA4348/2-1 to G.H.), Kinderherzen e.V. (W-H-001-2014 to G.H.), and Stiftung KinderHerz (2511-6-13 to G.H.).

Received: August 27, 2016
Revised: December 21, 2016
Accepted: March 20, 2017
Published: May 2, 2017

REFERENCES

Akhurst, R.J., and Hata, A. (2012). Targeting the TGFβ signalling pathway in disease. Nat. Rev. Drug Discov. *11*, 790–811.

Alarcón, C., Zaromytidou, A.-I., Xi, Q., Gao, S., Yu, J., Fujisawa, S., Barlas, A., Miller, A.N., Manova-Todorova, K., Macias, M.J., et al. (2009). Nuclear CDKs drive Smad transcriptional activation and turnover in BMP and TGF-beta pathways. Cell *139*, 757–769.

Ameshima, S., Golpon, H., Cool, C.D., Chan, D., Vandivier, R.W., Gardai, S.J., Wick, M., Nemenoff, R.A., Geraci, M.W., and Voelkel, N.F. (2003). Peroxisome proliferator-activated receptor gamma (PPARgamma) expression is decreased in pulmonary hypertension and affects endothelial cell growth. Circ. Res. *92*, 1162–1169.

Banks, A.S., McAllister, F.E., Camporez, J.P.G., Zushin, P.-J.H., Jurczak, M.J., Laznik-Bogoslavski, D., Shulman, G.I., Gygi, S.P., and Spiegelman, B.M. (2015). An ERK/Cdk5 axis controls the diabetogenic actions of PPARγ. Nature *517*, 391–395.

Barnes, J.W., Kucera, E.T., Tian, L., Mellor, N.E., Dvorina, N., Baldwin, W.W., 3rd, Aldred, M.A., Farver, C.F., Comhair, S.A.A., Aytekin, M., and Dweik, R.A. (2016). Bone morphogenic protein type 2 receptor mutation-independent mechanisms of disrupted bone morphogenetic protein signaling in idiopathic pulmonary arterial hypertension. Am. J. Respir. Cell Mol. Biol. *55*, 564–575.

Bertero, T., Lu, Y., Annis, S., Hale, A., Bhat, B., Saggar, R., Saggar, R., Wallace, W.D., Ross, D.J., Vargas, S.O., et al. (2014). Systems-level regulation of microRNA networks by miR-130/301 promotes pulmonary hypertension. J. Clin. Invest. *124*, 3514–3528.

Boucher, P., Li, W.-P., Matz, R.L., Takayama, Y., Auwerx, J., Anderson, R.G.W., and Herz, J. (2007). LRP1 functions as an atheroprotective integrator of TGFbeta and PDFG signals in the vascular wall: implications for Marfan syndrome. PLoS ONE *2*, e448.

Brock, M., Trenkmann, M., Gay, R.E., Michel, B.A., Gay, S., Fischler, M., Ulrich, S., Speich, R., and Huber, L.C. (2009). Interleukin-6 modulates the expression of the bone morphogenic protein receptor type II through a novel STAT3-microRNA cluster 17/92 pathway. Circ. Res. *104*, 1184–1191.

Calvier, L., Miana, M., Reboul, P., Cachofeiro, V., Martinez-Martinez, E., de Boer, R.A., Poirier, F., Lacolley, P., Zannad, F., Rossignol, P., and López-Andrés, N. (2013). Galectin-3 mediates aldosterone-induced vascular fibrosis. Arterioscler. Thromb. Vasc. Biol. *33*, 67–75.

Calvier, L., Martinez-Martinez, E., Miana, M., Cachofeiro, V., Rousseau, E., Sádaba, J.R., Zannad, F., Rossignol, P., and López-Andrés, N. (2015). The impact of galectin-3 inhibition on aldosterone-induced cardiac and renal injuries. JACC Heart Fail. *3*, 59–67.

Chen, N.-Y., D Collum, S., Luo, F., Weng, T., Le, T.T., M Hernandez, A., Philip, K., Molina, J.G., Garcia-Morales, L.J., Cao, Y., et al. (2016). Macrophage bone morphogenic protein receptor 2 depletion in idiopathic pulmonary fibrosis and group III pulmonary hypertension. Am. J. Physiol. Lung Cell. Mol. Physiol. *311*, L238–L254.

Deuse, T., Hua, X., Wang, D., Maegdefessel, L., Heeren, J., Scheja, L., Bolaños, J.P., Rakovic, A., Spin, J.M., Stubbendorff, M., et al. (2014). Dichloroacetate prevents restenosis in preclinical animal models of vessel injury. Nature *509*, 641–644.

Diebold, I., Hennigs, J.K., Miyagawa, K., Li, C.G., Nickel, N.P., Kaschwich, M., Cao, A., Wang, L., Reddy, S., Chen, P.-I., et al. (2015). BMPR2 preserves mitochondrial function and DNA during reoxygenation to promote endothelial cell survival and reverse pulmonary hypertension. Cell Metab. *21*, 596–608.

Dormandy, J., Bhattacharya, M., and van Troostenburg de Bruyn, A.-R.; PROactive investigators (2009). Safety and tolerability of pioglitazone in high-risk patients with type 2 diabetes: an overview of data from PROactive. Drug Saf. *32*, 187–202.

Falcetti, E., Hall, S.M., Phillips, P.G., Patel, J., Morrell, N.W., Haworth, S.G., and Clapp, L.H. (2010). Smooth muscle proliferation and role of the prostacyclin (IP) receptor in idiopathic pulmonary arterial hypertension. Am. J. Respir. Crit. Care Med. *182*, 1161–1170.

Feng, F., Harper, R.L., and Reynolds, P.N. (2016). BMPR2 gene delivery reduces mutation-related PAH and counteracts TGF-β-mediated pulmonary cell signalling. Respirology *21*, 526–532.

Galiè, N., Humbert, M., Vachiery, J.-L., Gibbs, S., Lang, I., Torbicki, A., Simonneau, G., Peacock, A., Vonk Noordegraaf, A., Beghetti, M., et al. (2016). 2015 ESC/ERS guidelines for the diagnosis and treatment of pulmonary hypertension: The Joint Task Force for the Diagnosis and Treatment of Pulmonary Hypertension of the European Society of Cardiology (ESC) and the European Respiratory Society (ERS): Endorsed by: Association for European Paediatric and Congenital Cardiology (AEPC), International Society for Heart and Lung Transplantation (ISHLT). Eur. Heart J. *37*, 67–119.

Guignabert, C., Alvira, C.M., Alastalo, T.-P., Sawada, H., Hansmann, G., Zhao, M., Wang, L., El-Bizri, N., and Rabinovitch, M. (2009). Tie2-mediated loss of peroxisome proliferator-activated receptor-gamma in mice causes PDGF receptor-beta-dependent pulmonary arterial muscularization. Am. J. Physiol. Lung Cell. Mol. Physiol. *297*, L1082–L1090.

Hansmann, G., and Rabinovitch, M. (2010). The protective role of adiponectin in pulmonary vascular disease. Am. J. Physiol. Lung Cell. Mol. Physiol. *298*, L1–L2.

Hansmann, G., and Zamanian, R.T. (2009). PPARgamma activation: a potential treatment for pulmonary hypertension. Sci. Transl. Med. *1*, 12ps14.

Hansmann, G., de Jesus Perez, V.A., Alastalo, T.-P., Alvira, C.M., Guignabert, C., Bekker, J.M., Schellong, S., Urashima, T., Wang, L., Morrell, N.W., and Rabinovitch, M. (2008). An antiproliferative BMP-2/PPARgamma/apoE axis in human and murine SMCs and its role in pulmonary hypertension. J. Clin. Invest. *118*, 1846–1857.

Hansmann, G., Fernandez-Gonzalez, A., Aslam, M., Vitali, S.H., Martin, T., Mitsialis, S.A., and Kourembanas, S. (2012). Mesenchymal stem cell-mediated reversal of bronchopulmonary dysplasia and associated pulmonary hypertension. Pulm. Circ. *2*, 170–181.

Hassoun, P.M., Mouthon, L., Barberà, J.A., Eddahibi, S., Flores, S.C., Grimminger, F., Jones, P.L., Maitland, M.L., Michelakis, E.D., Morrell, N.W., et al. (2009). Inflammation, growth factors, and pulmonary vascular remodeling. J. Am. Coll. Cardiol. *54* (1, Suppl), S10–S19.

Hatta, M., and Cirillo, L.A. (2007). Chromatin opening and stable perturbation of core histone:DNA contacts by FoxO1. J. Biol. Chem. *282*, 35583–35593.

Heinz, S., Benner, C., Spann, N., Bertolino, E., Lin, Y.C., Laslo, P., Cheng, J.X., Murre, C., Singh, H., and Glass, C.K. (2010). Simple combinations of lineage-determining transcription factors prime cis-regulatory elements required for macrophage and B cell identities. Mol. Cell *38*, 576–589.

Hopper, R.K., Moonen, J.-R.A.J., Diebold, I., Cao, A., Rhodes, C.J., Tojais, N.F., Hennigs, J.K., Gu, M., Wang, L., and Rabinovitch, M. (2016). In pulmonary arterial hypertension, reduced BMPR2 promotes endothelial-to-mesenchymal transition via HMGA1 and its target slug. Circulation *133*, 1783–1794.

Humbert, M., Sitbon, O., Chaouat, A., Bertocchi, M., Habib, G., Gressin, V., Yaïci, A., Weitzenblum, E., Cordier, J.-F., Chabot, F., et al. (2010). Survival in patients with idiopathic, familial, and anorexigen-associated pulmonary arterial hypertension in the modern management era. Circulation *122*, 156–163.

Jonigk, D., Al-Omari, M., Maegel, L., Müller, M., Izykowski, N., Hong, J., Hong, K., Kim, S.-H., Dorsch, M., Mahadeva, R., et al. (2013). Anti-inflammatory and immunomodulatory properties of α1-antitrypsin without inhibition of elastase. Proc. Natl. Acad. Sci. USA *110*, 15007–15012.

Kernan, W.N., Viscoli, C.M., Furie, K.L., Young, L.H., Inzucchi, S.E., Gorman, M., Guarino, P.D., Lovejoy, A.M., Peduzzi, P.N., Conwit, R., et al.; IRIS Trial Investigators (2016). Pioglitazone after ischemic stroke or transient ischemic attack. N. Engl. J. Med. *374*, 1321–1331.

Landt, S.G., Marinov, G.K., Kundaje, A., Kheradpour, P., Pauli, F., Batzoglou, S., Bernstein, B.E., Bickel, P., Brown, J.B., Cayting, P., et al. (2012). ChIP-seq guidelines and practices of the ENCODE and modENCODE consortia. Genome Res. *22*, 1813–1831.

Li, H., and Durbin, R. (2010). Fast and accurate long-read alignment with Burrows-Wheeler transform. Bioinformatics *26*, 589–595.

Li, H., Handsaker, B., Wysoker, A., Fennell, T., Ruan, J., Homer, N., Marth, G., Abecasis, G., and Durbin, R.; 1000 Genome Project Data Processing Subgroup (2009). The Sequence Alignment/Map format and SAMtools. Bioinformatics *25*, 2078–2079.

Li, G., Tang, L., Jia, P., Zhao, J., Liu, D., and Liu, B. (2016). Elevated plasma connective tissue growth factor levels in children with pulmonary arterial hypertension associated with congenital heart disease. Pediatr. Cardiol. *37*, 714–721.

Lin, L.-C., Hsu, S.-L., Wu, C.-L., Liu, W.-C., and Hsueh, C.-M. (2011). Peroxisome proliferator-activated receptor γ (PPARγ) plays a critical role in the development of TGFβ resistance of H460 cell. Cell. Signal. *23*, 1640–1650.

Loke, Y.K., Kwok, C.S., and Singh, S. (2011). Comparative cardiovascular effects of thiazolidinediones: systematic review and meta-analysis of observational studies. BMJ *342*, d1309.

Long, L., Crosby, A., Yang, X., Southwood, M., Upton, P.D., Kim, D.-K., and Morrell, N.W. (2009). Altered bone morphogenetic protein and transforming growth factor-beta signaling in rat models of pulmonary hypertension: potential for activin receptor-like kinase-5 inhibition in prevention and progression of disease. Circulation *119*, 566–576.

Long, L., Ormiston, M.L., Yang, X., Southwood, M., Gräf, S., Machado, R.D., Mueller, M., Kinzel, B., Yung, L.M., Wilkinson, J.M., et al. (2015). Selective enhancement of endothelial BMPR-II with BMP9 reverses pulmonary arterial hypertension. Nat. Med. *21*, 777–785.

Ma, W., Han, W., Greer, P.A., Tuder, R.M., Toque, H.A., Wang, K.K.W., Caldwell, R.W., and Su, Y. (2011). Calpain mediates pulmonary vascular remodeling in rodent models of pulmonary hypertension, and its inhibition attenuates pathologic features of disease. J. Clin. Invest. *121*, 4548–4566.

Macias, M.J., Martin-Malpartida, P., and Massagué, J. (2015). Structural determinants of Smad function in TGF-β signaling. Trends Biochem. Sci. *40*, 296–308.

Malenfant, S., Neyron, A.-S., Paulin, R., Potus, F., Meloche, J., Provencher, S., and Bonnet, S. (2013). Signal transduction in the development of pulmonary arterial hypertension. Pulm. Circ. *3*, 278–293.

Matsa, E., Burridge, P.W., Yu, K.-H., Ahrens, J.H., Termglinchan, V., Wu, H., Liu, C., Shukla, P., Sayed, N., Churko, J.M., et al. (2016). Transcriptome profiling of patient-specific human iPSC-cardiomyocytes predicts individual drug safety and efficacy responses in vitro. Cell Stem Cell *19*, 311–325.

Meloche, J., Courchesne, A., Barrier, M., Carter, S., Bisserier, M., Paulin, R., Lauzon-Joset, J.-F., Breuils-Bonnet, S., Tremblay, É., Biardel, S., et al. (2013). Critical role for the advanced glycation end-products receptor in pulmonary arterial hypertension etiology. J. Am. Heart Assoc. *2*, e005157.

Morrell, N.W. (2006). Pulmonary hypertension due to BMPR2 mutation: a new paradigm for tissue remodeling? Proc. Am. Thorac. Soc. *3*, 680–686.

Morrell, N.W., Bloch, D.B., ten Dijke, P., Goumans, M.-J.T.H., Hata, A., Smith, J., Yu, P.B., and Bloch, K.D. (2016). Targeting BMP signalling in cardiovascular disease and anaemia. Nat. Rev. Cardiol. *13*, 106–120.

Newman, J.H., Phillips, J.A., 3rd, and Loyd, J.E. (2008). Narrative review: the enigma of pulmonary arterial hypertension: new insights from genetic studies. Ann. Intern. Med. *148*, 278–283.

Paulin, R., Courboulin, A., Meloche, J., Mainguy, V., Dumas de la Roque, E., Saksouk, N., Côté, J., Provencher, S., Sussman, M.A., and Bonnet, S. (2011). Signal transducers and activators of transcription-3/pim1 axis plays a critical role in the pathogenesis of human pulmonary arterial hypertension. Circulation *123*, 1205–1215.

Pelham, C.J., Ketsawatsomkron, P., Groh, S., Grobe, J.L., de Lange, W.J., Ibeawuchi, S.-R.C., Keen, H.L., Weatherford, E.T., Faraci, F.M., and Sigmund, C.D. (2012). Cullin-3 regulates vascular smooth muscle function and arterial blood pressure via PPARγ and RhoA/Rho-kinase. Cell Metab. *16*, 462–472.

Ranchoux, B., Antigny, F., Rucker-Martin, C., Hautefort, A., Péchoux, C., Bogaard, H.J., Dorfmüller, P., Remy, S., Lecerf, F., Planté, S., et al. (2015). Endothelial-to-mesenchymal transition in pulmonary hypertension. Circulation *131*, 1006–1018.

Sanderson, N., Factor, V., Nagy, P., Kopp, J., Kondaiah, P., Wakefield, L., Roberts, A.B., Sporn, M.B., and Thorgeirsson, S.S. (1995). Hepatic expression of mature transforming growth factor beta 1 in transgenic mice results in multiple tissue lesions. Proc. Natl. Acad. Sci. USA *92*, 2572–2576.

Savai, R., Al-Tamari, H.M., Sedding, D., Kojonazarov, B., Muecke, C., Teske, R., Capecchi, M.R., Weissmann, N., Grimminger, F., Seeger, W., et al. (2014). Pro-proliferative and inflammatory signaling converge on FoxO1 transcription factor in pulmonary hypertension. Nat. Med. *20*, 1289–1300.

Selimovic, N., Bergh, C.-H., Andersson, B., Sakiniene, E., Carlsten, H., and Rundqvist, B. (2009). Growth factors and interleukin-6 across the lung circulation in pulmonary hypertension. Eur. Respir. J. *34*, 662–668.

Sheikh, A.Q., Lighthouse, J.K., and Greif, D.M. (2014). Recapitulation of developing artery muscularization in pulmonary hypertension. Cell Rep. *6*, 809–817.

Soccio, R.E., Chen, E.R., and Lazar, M.A. (2014). Thiazolidinediones and the promise of insulin sensitization in type 2 diabetes. Cell Metab. *20*, 573–591.

Soubrier, F., Chung, W.K., Machado, R., Grünig, E., Aldred, M., Geraci, M., Loyd, J.E., Elliott, C.G., Trembath, R.C., Newman, J.H., and Humbert, M. (2013). Genetics and genomics of pulmonary arterial hypertension. J. Am. Coll. Cardiol. *62* (25, Suppl), D13–D21.

Steiner, M.K., Syrkina, O.L., Kolliputi, N., Mark, E.J., Hales, C.A., and Waxman, A.B. (2009). Interleukin-6 overexpression induces pulmonary hypertension. Circ. Res. *104*, 236–244, 28p, 244.

Subramanian, V., Golledge, J., Heywood, E.B., Bruemmer, D., and Daugherty, A. (2012). Regulation of peroxisome proliferator-activated receptor-γ by angiotensin II via transforming growth factor-β1-activated p38 mitogen-activated protein kinase in aortic smooth muscle cells. Arterioscler. Thromb. Vasc. Biol. *32*, 397–405.

Sutendra, G., and Michelakis, E.D. (2014). The metabolic basis of pulmonary arterial hypertension. Cell Metab. *19*, 558–573.

Takata, Y., Kitami, Y., Yang, Z.-H., Nakamura, M., Okura, T., and Hiwada, K. (2002). Vascular inflammation is negatively autoregulated by interaction between CCAAT/enhancer-binding protein-delta and peroxisome proliferator-activated receptor-gamma. Circ. Res. *91*, 427–433.

Tuder, R.M., Archer, S.L., Dorfmüller, P., Erzurum, S.C., Guignabert, C., Michelakis, E., Rabinovitch, M., Schermuly, R., Stenmark, K.R., and Morrell, N.W. (2013). Relevant issues in the pathology and pathobiology of pulmonary hypertension. J. Am. Coll. Cardiol. *62* (25, Suppl), D4–D12.

Wang, L.H., Yang, X.Y., Zhang, X., Huang, J., Hou, J., Li, J., Xiong, H., Mihalic, K., Zhu, H., Xiao, W., and Farrar, W.L. (2004). Transcriptional inactivation of STAT3 by PPARgamma suppresses IL-6-responsive multiple myeloma cells. Immunity *20*, 205–218.

Wang, J., Yang, K., Xu, L., Zhang, Y., Lai, N., Jiang, H., Zhang, Y., Zhong, N., Ran, P., and Lu, W. (2013). Sildenafil inhibits hypoxia-induced transient receptor potential canonical protein expression in pulmonary arterial smooth muscle via cGMP-PKG-PPARγ axis. Am. J. Respir. Cell Mol. Biol. *49*, 231–240.

Wang, X., Liang, Z., Xu, X., Li, J., Zhu, Y., Meng, S., Li, S., Wang, S., Xie, B., Ji, A., et al. (2016). miR-148a-3p represses proliferation and EMT by establishing regulatory circuits between ERBB3/AKT2/c-myc and DNMT1 in bladder cancer. Cell Death Dis. *7*, e2503.

Weiske, J., and Huber, O. (2006). The histidine triad protein Hint1 triggers apoptosis independent of its enzymatic activity. J. Biol. Chem. *281*, 27356–27366.

Xu, P., Liu, J., and Derynck, R. (2012). Post-translational regulation of TGF-β receptor and Smad signaling. FEBS Lett. *586*, 1871–1884.

Yadav, H., Quijano, C., Kamaraju, A.K., Gavrilova, O., Malek, R., Chen, W., Zerfas, P., Zhigang, D., Wright, E.C., Stuelten, C., et al. (2011). Protection from obesity and diabetes by blockade of TGF-β/Smad3 signaling. Cell Metab. *14*, 67–79.

Yung, L.-M., Nikolic, I., Paskin-Flerlage, S.D., Pearsall, R.S., Kumar, R., and Yu, P.B. (2016). A Selective Transforming growth factor-β ligand trap attenuates pulmonary hypertension. Am. J. Respir. Crit. Care Med. *194*, 1140–1151.

Zaiman, A.L., Podowski, M., Medicherla, S., Gordy, K., Xu, F., Zhen, L., Shimoda, L.A., Neptune, E., Higgins, L., Murphy, A., et al. (2008). Role of the TGF-beta/Alk5 signaling pathway in monocrotaline-induced pulmonary hypertension. Am. J. Respir. Crit. Care Med. *177*, 896–905.

Zhang, Y., Liu, T., Meyer, C.A., Eeckhoute, J., Johnson, D.S., Bernstein, B.E., Nusbaum, C., Myers, R.M., Brown, M., Li, W., and Liu, X.S. (2008). Model-based analysis of ChIP-seq (MACS). Genome Biol. *9*, R137.

Zhang, Y., Xu, D., Huang, H., Chen, S., Wang, L., Zhu, L., Jiang, X., Ruan, X., Luo, X., Cao, P., et al. (2014). Regulation of glucose homeostasis and lipid metabolism by PPP1R3G-mediated hepatic glycogenesis. Mol. Endocrinol. *28*, 116–126.

STAR★METHODS

KEY RESOURCES TABLE

REAGENT or RESOURCE	SOURCE	IDENTIFIER
Antibodies		
vWF	Dako	Cat#A0082; RRID: AB_2315602
PCNA	Abcam	Cat#Ab29; RRID: AB_303394
Ki67	Cell Signaling	Cat#11882
Anti-mouse IgG	Life Technologies	Cat#A11001
Anti-rabbit IgG	Life Technologies	Cat#A21207
PhosphoSTAT3	Cell Signaling	Cat#9131; RRID: AB_331586
STAT3	Cell Signaling	Cat#9139; RRID: AB_331757
PhosphoSMAD3	Cell Signaling	Cat#9520; RRID: AB_2193207
SMAD3	Cell Signaling	Cat#9523; RRID: AB_2193182
PhosphoFoxO1	Cell Signaling	Cat#9464
FoxO1	Novus Biologocals	Cat#NB100-2312; RRID: AB_10000747
SMAD4	Santa Cruz	Cat#Sc-7966; RRID: AB_627905
PPARγ	Santa Cruz	Cat#sc-7273; RRID: AB_628115
TGFβ1	Abcam	Cat#Ab64715; RRID: AB_1144265
CTGF	Santa Cruz	Cat#sc-14939; RRID: AB_638805
αSMA	Sigma-Aldrich	Cat#A2547; RRID: AB_476701
α-Tubulin	Sigma-Aldrich	Cat#T 6074; RRID: AB_477582
PFKP	Cell Signaling	Cat#8164P
PPP1R3G	Abgent	Cat#AP11993b-AB
GAPDH	Santa Cruz	Cat#sc-25778; RRID: AB_10167668
Lamine B	Santa Cruz	Cat#sc-6216; RRID: AB_648156
Anti-rabbit IgG	NEB	Cat#7074S
Anti-mouse IgG	NEB	Cat#7076S
Chemicals, Peptides, and Recombinant Proteins		
GW9662	Sigma-Aldrich	Cat#M6191
Pioglitazone	Sigma-Aldrich	Cat#E6910
BMP2	Sigma-Aldrich	Cat#B3555
TGFβ1	R&D Systems	Cat#240-B-002
BP-1-102	Calbiochem	Cat#573132
PFKP	Origene	Cat# TP300673
Critical Commercial Assays		
MTT	ATCC	Cat#30-1010K
XF Cell Mito Stress Test kit	Seahorse Bioscience	Cat#103015-100
MitoPT JC-1 Assay kit	Immunochemistry Technologies	Cat#911
NE-PER nuclear and cytoplasmic extraction kit	Thermo Scientific	Cat#78833
Quantikine TGFβ1 ELISA kit	R&D Systems	Cat#MB100B
Low Cell# ChIP kit	Diagenode	Cat#C01010072
IPure kit	Diagenode	Cat#C03010014
Deposited Data		
PPARγ ChIP-seq data	This study	SRA: SRP099035
Smad3 ChIP-seq data	This study	SRA: SRP099035
Experimental Models: Cell Lines		
Primary human pulmonary artery smooth muscle cells	Lonza	Cat# CC-2581

(*Continued on next page*)

Continued		
REAGENT or RESOURCE	SOURCE	IDENTIFIER
Experimental Models: Organisms/Strains		
SM22α Cre PPARγ $^{flox/flox}$ mice	Hansmann et al., 2008	N/A
C57Bl/6-TgAlb/TGFβ1 mice	Sanderson et al., 1995	N/A
Oligonucleotides		
pre-miR-130a	Thermo Fisher Scientific	Cat#PM10506
pre-miR-331-5p	Thermo Fisher Scientific	Cat#PM11179
negative control miRNA precursor	Thermo Fisher Scientific	Cat#AM17110
antagomiR-130a mirVana	Thermo Fisher Scientific	Cat#4464084
negative control mirVana	Thermo Fisher Scientific	Cat#4464076
Recombinant DNA		
packaging plasmid	Origene	Cat#TR30022
pGFP-C-shLenti plasmid:	Origene	N/A
shScramble: 5′ GCACTACCAGAGCTAACTC AGATAGTACT 3‘	Origene	N/A
shLacZi: 5′ GCACTACCAGAGCTAACTCAG ATAGTACT 3‘	Origene	N/A
shPPARγi – Construct A: 5′ TGAGAAGA CTCAGCTCTACAATAAGCCTC 3′	Origene	N/A
shPPARγi – Construct B: 5′ TGACTTGAA CGACCAAGTAACTCTCCTCA 3′	Origene	N/A
Software and Algorithms		
ZEN software	Zeiss	N/A
ViiA7 software V1.2.2	Applied Biosystems	N/A
GraphPad Prism 7	GraphPad Software	N/A
Ingenuity Pathway Analysis (IPA)	QIAGEN	N/A
Image Lab Software	BioRad	N/A
BWA	Li and Durbin, 2010	https://sourceforge.net/projects/bio-bwa/files/
SAMtools	Li et al., 2009	https://sourceforge.net/projects/samtools/files/latest/download
MACS2	Zhang et al., 2008	https://github.com/taoliu/MACS
Irreproducible Discovery Rate (IDR) analysis methodology	Landt et al., 2012	https://sites.google.com/site/anshulkundaje/projects/idr
Homer	Heinz et al., 2010	http://homer.ucsd.edu/homer/

CONTACT FOR REAGENT AND RESOURCE SHARING

Further information and requests for resources and reagents should be directed to and will be fulfilled by the Lead Contact, Georg Hansmann, MD, PhD (georg.hansmann@gmail.com).

EXPERIMENTAL MODEL AND SUBJECT DETAILS

All animal studies were performed according to the institutional animal care and use guidelines and the according state regulations: Animal protocol numbers 13/1328 (Hannover) and XIV-I-001/2146/2012 (Budapest).

SM22α Cre PPARγ $^{flox/flox}$ mice (SMC PPARγ –/–)

We cross-bred SM22α promoter–driven Cre mice with PPARγ$^{flox/flox}$ mice (Jackson Laboratory), which resulted in SM22α Cre PPARγ$^{flox/flox}$ (SMC PPARγ −/−) mice, i.e., mice with targeted deletion of PPARγ in arterial smooth muscle cells (Hansmann et al., 2008). PCR conditions and primer information used for genotyping are available from Jackson Laboratory (Hansmann et al., 2008). We used 15 week-old male SMC PPARγ −/− (n = 5) and littermate control mice (n = 8). SMC PPARγ −/− mice at that age spontaneously have pulmonary arterial hypertension (PAH), right ventricular hypertrophy (RVH) and peripheral PA muscularization, as described previously (Hansmann et al., 2008).

Transgenic mice TG-TGFβ1 (C57Bl/6-TgAlb/TGF-β1) with systemic TGFβ1 overexpression

TGFβ1 transgenic mice were obtained from Dr. S. Thorgeirsson (National Cancer Institute/National Institutes of Health, Bethesda, MD) (Sanderson et al., 1995). Overexpression of active TGFβ1 is ensured by the porcine TGFβ1 transgene that is selectively expressed in hepatocytes under the control of murine albumin promoter and enhancer. In the TGFβ1 transgene, cysteine 223 and 225 were mutated to serine to destabilize the latent TGFβ1 molecule and promote secretion of active TGFβ1. All transgenic mice with elevated plasma TGFβ1 levels are male and all non-transgenic mice are female, suggesting that the transgene is on the Y chromosome (Sanderson et al., 1995). TGFβ1 mice on CBA × C57BL/6 F2 background were backcrossed to C57BL/6 strain for 20 generations. The newly generated C57Bl/6-TgAlb/TGFβ1 mice have homogeneous C57BL/6 genetic background. The control and transgenic males (TG-TGFβ1) were divided in 2 sets. A first set of 10-12 week-old control and TG-TGFβ1 mice (n = 3) underwent invasive hemodynamic measurement only (RV, LV and aorta catheterization in closed chest technique). A second set of 10-12 week old control and TG-TGFβ1 mice (n = 7-12) was treated for 5 weeks either with regular chow versus pioglitazone (20mg/kg/day) incorporated into the chow, and sacrificed at 15 to 17 weeks of age. In the second set of mice, invasive hemodynamic measurements (RV, LV, aortic catheterization) and tissue harvest were conducted after oral pioglitazone treatment for 5 weeks.

HPASMC isolation and culture

Commercially available human (female) pulmonary artery smooth muscle cells (HPASMC; CC-2581, Lonza) or directly isolated HPASMC were cultured in Smooth Muscle Cell Basal Medium (CC-31-81; Lonza) supplemented with 10% FBS and growth factors from SmGM-2 Single Quots (CC-4149; Lonza), 100 U/ml penicillin and 0.1 mg/ml streptomycin; (15140-122; GIBCO). Lung explant-derived HPASMC were isolated from pulmonary arteries obtained from patients with PAH or chronic obstructive pulmonary diseae (COPD). The adventitia was removed and segments of the pulmonary arteries were cut to expose the luminal surface. The endothelium was removed by gentle scraping with forceps. The medial explants were cut in small pieces, digested for 2 hr at 37°C in PBS (100100-015; GIBCO) with collagenase type II (1 mg/ml; 17101-015; GIBCO) and then transferred to T25 flasks with Smooth Muscle Cell Basal Medium. For in vitro experiments, the PASMC were used between passages 3 and 8.

Cell stimulations

HPASMC were serum starved (0.1% FBS) for 24h and then pre-incubated and stimulated as described in the figure legends, with a single or combination of the following drugs (unless specified differently in the figure legend): After 24h of starvation, cells were pre-incubated with GW9662 (1 μM; M6191; Sigma-Aldrich) or DMSO (vol. eq.; D2650; Sigma-Aldrich) for 1h, then with pioglitazone (10 μM; E6910; Sigma-Aldrich) or BMP2 (10ng/ml; B3555; Sigma-Aldrich) for another 24h. After 24h of starvation plus 24h of pre-incubation, cells were stimulated with recombinant TGFβ1 (5ng/ml; 240-B-002; R&D systems). Other pre-incubation/stimulations involving the Stat3 inhibitor BP-1-102 (10 μM; 573132; Calbiochem) or recombinant PFKP (100ng/ml; TP300673; Origene) were performed as described in the corresponding legends.

Human lung tissue samples

Human FFPE tissue specimens (retrieved from the archives of the Institute of Pathology of Hannover Medical School and fresh tissue materials for cell extractions (after LuTx performed at MHH) were handled anonymously, following the requirements of the ethics committee of Hannover Medical School (IRB #1691-2013, #3381-2016).

Human FFPE lung tissue samples used for laser capture microdissection (LCM)

Group	Gender	Age (years)	Diagnosis
Control (LuTx donor)	male	35	Downsizing lung
Control (LuTx donor)	male	60	Downsizing lung
Control (LuTx donor)	female	43	Downsizing lung
Control (LuTx donor)	female	12	Downsizing lung
Control (LuTx donor)	male	35	Downsizing lung
IPAH	male	10	IPAH
IPAH	female	47	IPAH
IPAH	female	36	IPAH
IPAH	female	48	IPAH
IPAH	female	53	IPAH

FFPE, formalin-fixed, paraffin-embedded; LuTx, lung transplantation; IPAH, idiopathic pulmonary arterial hypertension

METHOD DETAILS

Hemodynamic measurements

Measurements of RV pressure were performed under isoflurane anesthesia (1.5%–2.5%) applying a closed-chest technique in spontaneously breathing mice at 10-12 and 15-17 weeks of age, as previously described (Hansmann et al., 2008). Briefly, a 1.4 F microtip catheter (Millar Instruments, Houston, Texas) was inserted into the right jugular vein and then placed into the free RV cavity. 3-5 simultaneous tracings from different time points were taken to determine the individual RV variables such as heart rate, RVSP, RVEDP, RV dp/dt. Aortic and LV pressure were determined by catheterization via the right carotid artery under isoflurane anesthesia (1.5%–2.5%). Briefly, a 1.4F microtip catheter was inserted through the right carotid artery and advanced in the aortic arch, and then in a retrograde fashion past the aortic valve into the left ventricular cavity. The catheter was adjusted to lie in the free LV cavity/left ventricular outflow tract, and tracings were evaluated in real time to ensure adequate catheter placement. Systemic blood pressure was determined in the ascending aorta/the aortic arch, before the catheter was advanced into the LV. The pressures were recorded and analyzed using a PowerLab recording unit and LabChart software (AD Instruments, Colorado Springs, CO).

Tissue harvest and preparation

The chest was opened and abdominal aorta, inferior vena cava and left atrium were transected. The lungs were then perfused in vivo through the main pulmonary artery (MPA) by injecting 40ml normal saline into the beating RV. The perfused (white) left lung was isolated by ligation, cut and snap frozen for protein and RNA analysis. The right lung was tracheally injected with 10% formalin and as such inflated, fixed overnight, and then embedded in paraffin for histology. The MPA was carefully dissected, cleared from surrounding tissues and snap frozen in liquid nitrogen for further RNA analysis.

Lung histology / immunohistochemistry

Murine lung sections (5μm-thick, 2 step sections 200 μm apart) were deparaffinized in xylene and rehydrated. Immunohistochemical staining was performed by incubating tissue glas slides with the indicated primary antibody overnight at 4°C, after 1 hr of blocking at room temperature, according to the manufacturer's instructions. Secondary antibodies and peroxidase staining was performed according to manufacturer's instructions (Vector laboratories). Slides were counterstained with Hematoxylin. Other sections were also stained with Masson's trichrome for collagen.

Human lung sections were obtained from 4 IPAH patients (lung explantat tissue) and compared to 3 donors (obtained from healthy down-sized lung explant tissue). The protocol for tissue processing and sectioning was the same as for murine lung.

Pulmonary vascular morphometry and quantification

Peripheral vascularization was determined by counting the number of von Willebrand (vWF)-positive vessels in 15 randomly taken images (without bronchi / bronchioles in the field) per animal at 200 × magnification, stratified by diameter (< 50 and 50–100 μm), using ImageJ software as described previously (Hansmann et al., 2012). αSMA-positive staining was quantified in vessels less than 100 μm outer diameter in 15 sections per animal, captured at 400 × magnification (Hansmann et al., 2012). The wall thickness was measured using ImageJ software and compared between groups using the following equation (Hansmann et al., 2012): Medial thickness index = $[(area_{ext} - area_{int})/area_{ext}]$, where $area_{ext}$ and $area_{int}$ are the areas within the external and internal boundaries of the α-SMA layer, respectively. The media staining (CTGF or αSMA) was measured accordingly from 15 images. Per vessel, the ratio of the stained surface in the media to the total media area was measured with ImageJ software to evaluate the percentage of staining. Taking the images and quantifications were done blinded, by 2 persons.

Lentiviral small hairpin RNA interference (shRNAi) gene silencing (stable knockdown)

For longterm gene silencing of PPARγ (4 variants), a lentivirus with an integrated shRNA was used. Scramble shRNA or a shRNA against LacZ were used as negative controls.

shScramble: 5′ GCACTACCAGAGCTAACTCAGATAGTACT 3′
shLacZi: 5′ GCACTACCAGAGCTAACTCAGATAGTACT 3′
shPPARγi – Construct A: 5′ TGAGAAGACTCAGCTCTACAATAAGCCTC 3′
shPPARγi – Construct B: 5′ TGACTTGAACGACCAAGTAACTCTCCTCA 3′

These constructs were designed by Origene in a pGFP-C-shLenti plasmid. First, the lentiviral particles were produced by transfecting HEK293T with shRNA plasmid and the packaging plasmid (TR30022; Origene), according to the manufacter's protocol. Then, HPASMC were seeded in $25cm^2$ flask and then incubated with 500 μL of HEK293T supernatant containing the lentiviral particles supplemented with polybrene (8 μg/mL; 107689, Sigma-Aldrich) for 6h. The cells were allowed to recover for 48h, followed by selection with puromycin (Sigma-Aldrich) at 0,5 μg/ml for 7-10 days. The shRNA PPARγ construct with the lower knockdown efficiency (approx. 70% knockdown of mRNA and protein) was used on purpose for ChIP experiments with BMP2 stimulation (construct B, Figure S3), so that PPARγ could still be pulled down. For experiments others than ChIP, construct A (approx. 70% knockdown of RNA and protein) was used.

Transient transfection with pre-miR or antagomiR

3×10^4 HPASMC / well were seeded in 12-well-plates overnight. Cells were transfected in 1ml of Smooth Muscle Cell Basal Medium with Lipofectamine RNAiMax reagent (13778; Thermo Fischer Scientific) with 30nM of pre-miR-130a miRNA (PM10506; Thermo Fischer Scientific), pre-miR-331-5p (PM11179; Thermo Fischer Scientific), negative control miRNA precursor (AM17110; Thermo Fischer Scientific), antagomiR-130a mirVana miRNA inhibitor (4464084; Thermo Fischer Scientific) or negative control mirVana miRNA inhibitor (4464076; Thermo Fischer Scientific), according to the manufacturer's instructions.

Immunofluorescence

$2.5x10^4$ HPASMC / chamber were seeded in Lab-Tek 4-chamber slides (154526; Thermo Fisher Scientific) and allowed to adhere overnight. After stimulations, cells were washed with PBS, fixated, and incubated with antibodies according to the manufacturer's recommendations. For mounting, antifade-DAPI (P36931; Life Technologies) was given on the coverslips, and slides were sealed with DPX (06522; Sigma-Aldrich). Images were acquired on a Zeiss AXIO fluorescence microscope. Images were processed with ZEN software (Zeiss). Random areas were picked in a blinded fashion, and a minimum of 500 nuclei per chamber were counted.

Ki67 measurement: Per image, the total number of nucleus (DAPI stained) were counted manually; the nucleus was considered KI67 positive when the KI67 staining overlapped the DAPI staining on merged images. The results are expressed as number of Ki67 positive nuclei over total number of nuclei. Each condition was repeated 3 times per experiment.

Cell Counts / Crystal violet staining and quantification

HPASMC were seeded at $2.5x10^4$ cells per well of a 24-well plate in 500μl of growth medium and allowed to adhere overnight. After stimulation, cells were washed with PBS, fixed with 4% paraformaldehyde, washed with PBS, stained with Crystal Violet (V5265; Sigma-Aldrich) 0,02% in 10% ethanol for 30 min, washed with distilled water and allowed to dry. A Zeiss AXIO transmitted light microscope was used to take images which were further processed with ZEN software (Zeiss). In each well, all the cells in a pre-defined square of 5mm x 5mm were counted. To confirm the counting results, the crystal violet was dissolved in 70% ethanol and the OD was measure at 590 nm in a microtiter plate reader. Counting and staining yielded similar results. Each condition was repeated 8 times per experiment.

MTT assay (cell proliferation)

HPASMC were seeded at $3x10^3$ cells per well of a 96-well plate in 200μl of growth medium and allowed to adhere overnight. After stimulation, the MMT (3-(4,5-dimethylthiazol-2-yl)-2,5-diphenyltetrazolium bromide) assay was performed according to the manufacturer's instructions (30-1010K; ATCC). The absorbance was measured in a microtiter plate reader (Multi detection system, Promega) at 570nm the next day, as a surrogate for cell proliferation. Each condition was repeated 8 times per experiment.

Mitochondrial respiration

Mitochondrial respiration was determined by measuring the oxygen consumption rate (OCR) with the XF Cell Mito Stress Test kit (103015-100; Seahorse Bioscience) in with a Seahorse XF24 Extracellular Flux Analyzer, according to the manufacturer's instructions. Briefly, HPASMC were serum starved (0.5% FBS) for 24h with vehicle (DMSO vol./vol. equivalent; D2650; Sigma-Aldrich) or pioglitazone (10 μM; E6910; Sigma-Aldrich). After 24h of simultaneous serum starvation plus pre-incubation, cells were stimulated with recombinant TGFβ1 (5 ng/ml; 240-B-002; R&D systems) for another 24h.

Mitochondrial transmembrane potential

Mitochondrial transmembrane potential was determined by measuring the JC-1 fluorescence with the MitoPT JC-1 Assay Kit (911; Immunochemistry Technologies), according to the manufacturer's instructions. HPASMC were stimulated as described in the "mitochondrial respiration" method. The JC-1 catonic dye exhibits potential-dependent accumulation in mitochondria, indicated by a fluorescence emission shift from green (~529 nm) to red (~590 nm). Therefore, the results are expressed as a ratio of 600/527 fluorescence measured by a Glomax Multi Detection System (Promega) plate reader.

Nuclear / Cytoplasmic extraction

Subcellular fractions (nuclear and cytoplasmic extracts) were performed using the NE-PER nuclear and cytoplasmic extraction reagents (78833; Thermo Scientific) and according the manufacturer's recommendations.

Co-Immunoprecipitation (CoIP)

CoIP on total cell lysate or on subcellular fractions (nuclear and cytoplasmic extracts) were performed using magnetic (8740; Cell signaling) or agarose beads (9007; Cell signaling) respectively, and performed according to the manufacturer's instructions. Before the Co-IP, protein concentration was measured by the Lowry protein assay (500-0113, 500-0114, 500-0115; Bio-Rad) and equal amount of protein was used per IP. After completion of the Co-IP, equal sample volumes were analyzed by western blot as described below. The antibodies used are anti-PPARγ (sc-7273X; E8 ChIP grade; Santa Cruz) and the negative control IgG (5415; Cell signaling).

Western blot

Cell lysates or tissue pieces were prepared by adding the lysis buffer Complete Lysis-M EDTA-free (04 719 964 001; Roche), supplemented with phosphatase inhibitor cocktail PhosphoSTOP EASYpack (04906845001; Roche) to the cells, scraping into a 1.5ml tube and centrifuging for 10 min at 12000 rpm. From the cell lysates or the nuclear / cytoplasmic extracts, protein concentrations were determined by the Lowry protein assay (500-0113, 500-0114, 500-0115; Bio-Rad). Equal amounts of protein were loaded into each lane of a 4%–12% Bis-Tris gel (Invitrogen) and subjected to electrophoresis under reducing conditions. After blotting, PVDF-membranes (Invitrogen) were blocked for 1h (milkpowder 5% in TBS/tween 0.1%–0.2%) and incubated with primary antibodies. Binding of secondary HRP-antibodies were visualized by ECL or ECL plus chemiluminescent (Amersham, Princeton, NJ). After densitometric analyses, optical density values were expressed as arbitrary units and normalized for protein loading, as described in the figure legends.

ELISA

Determination of plasma TGFβ1 levels: Blood samples were obtained by retro-orbital puncture and measured according to the Quantikine TGFβ1 ELISA kit protocol (R&D Systems). Briefly, samples were collected using siliconized microcentrifuge tubes (Sigma-Aldrich) and low-binding pipette tips (Sigma-Aldrich). EDTA was added at a final concentration of 1 mg/ml, and blood samples were first centrifuged at 1000xg for 20min to isolate plasma. A final centrifuge step at 10,000xg for 10min was also applied to sediment thrombocytes in plasma samples. Finally, 10μl of supernatants were used in the ELISA protocol.

RT-qPCR

Total RNA was extracted from cells or tissue pieces according to the TRIzol protocol (TRIzol, Life Technologies). RNA concentrations were measured spectrophotometrically (Nanopdrop 2000c; Thermo Scientific). For RNA, first strand cDNA was synthesized using SuperScript III enzyme according to the manufactuer's instructions (11752; Life Technologies). Quantitative PCR reaction was then performed with TaqMan probes using the SensiFAST Probe Lo-ROX Mix (BIO-84020; Bioline) according to the manufactuer's instructions. For each sample, multiplexed reaction was performed, for the target gene (with FAM reporter) and the housekeepers B2M or RPS9 (with VIC reporter). For microRNA (miR), first strand cDNA was synthesized using the TaqMan MicroRNA Reverse Transcription Kit according to the manufacturer's instructions (4366596; Life Technologies). Quantitative PCR reaction was then performed with TaqMan probes using the TaqMan Universal Master Mix II (4440046; Life Technologies) according to the manufacturer's instructions. miR-320 was used as housekeeper for human cells or tissues. Relative quantity (RQ) values were calculated using the ViiA7 software V1.2.2 (Applied Biosystems).

Sequence-based reagents

REAGENT or RESOURCE	SOURCE	IDENTIFIER
PPARg primers	Life Technologies	Cat#Hs01115513_m1
TGFb1 primers	Life Technologies	Cat#Hs00998133_m1
CTGF primers	Life Technologies	Cat#Hs01026927_g1
ACTA2 primers	Life Technologies	Cat#Hs00426835_g1
B2M primers	Life Technologies	Cat#Hs00984230_m1
Pparg primers	Life Technologies	Cat#Mm01184322_m1
Tgfb1 primers	Life Technologies	Cat#Mm0117820_m1
Ctgf primers	Life Technologies	Cat#Mm01192932_g1
Acta2 primers	Life Technologies	Cat#Mm01204962-gH
Rps9 primers	Life Technologies	Cat#Mm00850060_s1
hsa-miR-130a primers	Life Technologies	Cat#000454
hsa-miR-301b primers	Life Technologies	Cat#000528
hsa-miR-331-5p primers	Life Technologies	Cat#002233
hsa-miR-148a primers	Life Technologies	Cat#000470
hsa-miR-320 primers	Life Technologies	Cat#002277

Laser capture microdissection (LCM)

Five μm-thick FFPE serially cut tissue sections were mounted on a poly-L-lysine–coated membrane fixed onto a metal frame. After deparaffinization and counterstaining with hematoxylin, pulmonary arteries < 500 μm were isolated using the CellCut Plus system (MMI Molecular Machines and Industries AG). mRNA was isolated as recently described (Jonigk et al., 2013). From each compartment approximately 5,000 cells were harvested. mRNA cDNA synthesis (High-Capacity cDNA Reverse Transcription Kit; ThermoFisher Scientific) and pre-amplification with target gene–specific PCR primers (PreAmp Master Mix Kit; ThermoFisher

Scientific) were performed as reported previously (Jonigk et al., 2013). The pre-amplified cDNA was evaluated by qPCR as described further.

Chromatin immunoprecipitation (ChIP) and DNA sequencing

After 36h of starvation (DMEM, 0.5% FBS, penicillin/streptomycin), quiescent HPASMC were incubated with BMP2 (10ng/ml) for 10min or TGFβ1 (5ng/ml) for 30min. ChIP was performed using the Low Cell# ChIP kit (C01010072; Diagenode) according to the manufacturer's instructions with minor modifications described by Weiske and Huber (Weiske and Huber, 2006). First, antibodies directed against the proteins of interest (PPARγ: sc-7273X; Santa Cruz; Smad3, 9523, Cell signaling) and IgG (Diagenode) were bound to magnetic beads. During the nidning process, cells were fixed with 2mM disuccinimidyl glutarate (Sigma) for 45min at room temperature. Subsequently, the cells were washed twice with PBS. Chromatin was cross-linked for 7min at room temperature using 1% formaldehyde and washed twice with ice-cold PBS. The cross-linking reaction was stopped by incubation with glycine at a final concentration of 0.125M for 5min at room temperature. The cells were washed with ice-cold PBS and scraped from the cell culture dish in PBS and centrifuged. Each cell pellet was resuspended in a detergent-containing buffer, and chromatin was sheared by controlled sonification using the Covaris S2 sonicator. The sheared chromatin was divided into several aliquots depending on the number of antibodies which were used, plus input control followed by incubation with the antibody-coated beads overnight. The beads with bound antibody-protein-DNA complexes were washed and double stranded (ds) DNA was collected using the IPure kit (C03010014; Diagenode).

The dsDNA samples were sent to Diagenode for library preparation and sequencing. The Chip-seq Illumina reads were quality-checked using fastqc (http://www.bioinformatics.babraham.ac.uk/projects/fastqc/) and aligned to the GRCh38 human genome reference using BWA (Li and Durbin, 2010). Reads that either did not map, were not a part of primary alignment, failed platform/vendor quality checks, or had mapping quality less than 30 were removed from the alignments using SAMtools (Li et al., 2009) (samtools view -F 780 -q 30). The peaks were called using MACS2 (Zhang et al., 2008) and analyzed according to ENCODE's Irreproducible Discovery Rate (IDR) analysis methodology as described (Landt et al., 2012). Conservative sets of peaks were generated by setting the N_{max} limit on the number of most significant peaks in the pooled samples, where N_{max} was the maximum number of significant peaks at IDR = 0.04 in pairwise comparisons of three replicates for each condition. These conservative sets of peaks were analyzed using the annotatePeaks.pl and findMotifsGenome.pl utilities in Homer (Heinz et al., 2010).

QUANTIFICATION AND STATISTICAL ANALYSIS

For cell culture, each condition was tested at least in triplicates, and all experiments were repeated at least 3 times at different passages, and in cells from at least two different donors (unless specified differently). Values from multiple experiments are expressed as mean ± SEM. Normality was tested using the Kolmogorov-Smirnov test. Statistical significance was determined for multiple comparisons using one-way analysis of variance (ANOVA) followed by Bonferroni's multiple comparison (for normal distribution) or Kruskal-Wallis (for non-normal distribution) test. Student's t test was used for comparisons of two groups. $p < 0.05$ was considered significant.

DATA AND SOFTWARE AVAILABILITY

Data Resources

PPARγ ChIP-seq data and Smad3 ChIP-seq data have been deposited in the Sequence Read Archive under accession number SRA: SRP099035.